Erratum

Obaid, A. L., Nelson, M. E., Lindstrom, J. and Salzberg, B. M. (2005). Optical studies of nicotinic acetylcholine receptor subtypes in the guinea-pig enteric nervous system. *J. Exp. Biol.* **208**, 2981-3001.

In the original published on-line version of this paper, the acceptance date was incorrect. It should have read 2 June 2005. The error has been rectified and the current on-line version and print versions are correct.

We apologise to authors and readers for any inconvenience this may have caused.

The Journal of Experimental Biology 208, 2981-3001
Published by The Company of Biologists 2005
doi:10.1242/jeb.01732

Optical studies of nicotinic acetylcholine receptor subtypes in the guinea-pig enteric nervous system

A. L. Obaid[1], M. E. Nelson[1], J. Lindstrom[1] and B. M. Salzberg[1,2,*]

[1]*Department of Neuroscience* and [2]*Department of Physiology, University of Pennsylvania School of Medicine, Philadelphia, PA 19104-6074, USA*

*Author for correspondence (e-mail: bmsalzbe@mail.med.upenn.edu)

Accepted 2 June 2005

Summary

Nicotinic transmission in the enteric nervous system (ENS) is extensive, but the role of individual nicotinic acetylcholine receptor (nAChR) subtypes in the functional connectivity of its plexuses has been elusive. Using monoclonal antibodies (mAbs) against neuronal α3-, α4-, α3/α5-, β2-, β4- and α7-subunits, combined with radioimmunoassays and immunocytochemistry, we demonstrate that guinea-pig enteric ganglia contain all of these nAChR-subunits with the exception of α4, and so, differ from mammalian brain. This information alone, however, is insufficient to establish the functional role of the identified nAChR-subtypes within the enteric networks and, ultimately, their specific contributions to gastrointestinal physiology. We have used voltage-sensitive dyes and a high-speed CCD camera, in conjunction with specific antagonists to various nAChRs, to elucidate some of the distinct contributions of the individual subtypes to the behaviour of enteric networks. In the guinea-pig, the submucous plexus has the extraordinary advantage that it is virtually two-dimensional, permitting optical recording, with single cell resolution, of the electrical activity of *all* of its neurones. In this plexus, the block of α3β2-, α3β4- and/or α7-nAChRs always results in a decrease in the magnitude of the synaptic response. However, the magnitude of the fast excitatory post-synaptic potentials (epsps) evoked by electrical stimulation of a neighbouring ganglion varies from cell to cell, reflecting the differential expression of subunits already observed using mAbs, as well as the strengths of the activated synaptic inputs. At the same time, we observe that submucous neurones have a substantial mecamylamine (Mec)-insensitive (non-nicotinic) component to their fast epsps, which may point to the presence of purinergic or serotonergic fast epsps in this system. In the myenteric plexus, on the other hand, the antagonist-induced changes in the evoked synaptic response vary depending upon the location of the stimulating electrode with respect to the ganglion under study. The range of activity patterns that follows sequential pharmacological elimination of individual subtypes suggests that nAChRs may be capable of regulating the activity of both excitatory and inhibitory pathways, in a manner similar to that described in the central nervous system.

Key words: submucous plexus, myenteric plexus, high-speed optical recording, voltage-sensitive dye.

Introduction

Decoding the structure and function of native nicotinic acetylcholine receptors (nAChRs) is complex. Although the expression of defined combinations of nAChR-subunits in *Xenopus* oocytes permits the comparison of pharmacological properties of individual nAChR-subtypes, single neurones often express more than one subtype, making the physiological roles of nAChRs in intact neuronal networks difficult to assess (Colquhoun and Patrick, 1997). The function of a given nAChR depends upon its pre-, post- or peri-synaptic location as well as the activity of neighbouring non-nicotinic receptors. In addition, the properties of any neuronal ensemble depend not only on the intrinsic conductances of its neurones and the specific attributes of its many synapses but also on the complex and nonlinear dynamic interactions that result from the multiple parallel connectivity of its component cells (Parsons et al., 1991). Therefore, to understand nicotinic responses at the network level, it is necessary to record at high spatial and temporal resolution to characterize the behaviour of individual neurones and at lower spatial resolution to capture a panoramic view of network activity and to assess the directionality of the nicotinic pathways along the circumferential as well as the longitudinal axes.

The enteric nervous system (ENS) regulates most gastrointestinal functions. Its neurones are clustered in ganglia that interconnect to form distinct plexuses in the gut wall: the myenteric plexus lies between the longitudinal and circular muscle layers, and the submucous plexus between the circular muscle layer and the mucosa. The behaviour of the effector

systems in the gut (transporting epithelium, neuroendocrine cells, immune elements, blood vessels and smooth muscle) is controlled by both of these networks acting in concert. Therefore, a detailed knowledge of synaptic interactions within and between ganglia, and between the plexuses, is essential for understanding both normal and pathological gastrointestinal function. Because the ENS contains a limited number of functional elements that are located within simple quasi-two-dimensional structures, it is well suited for the analysis of intact circuits and their molecular components using multiple site optical recording of transmembrane voltage (MSORTV) combined with immunocytochemistry (Neunlist et al., 1999; Obaid et al., 1999a, 1992; Schemann et al., 2002). By virtue of its geometry, its transparency and its organization into small ganglia containing large neurones arrayed in a single optical plane, the submucous plexus of the guinea-pig is an optimal preparation in which to examine the dynamics of neuronal assemblies with single cell resolution and to understand how individual nAChR-subtypes interact to generate the normal patterning of activity as well as aberrations of these patterns. The myenteric plexus of the guinea-pig, on the other hand, although its ganglia are larger and more complex, has its own set of advantages, including the quasi-crystalline regularity of its supra-ganglionic architecture, which hints at the intrinsic directionality of the major gastrointestinal reflexes. In both of these mammalian neuronal networks, MSORTV permits monitoring of *many* neurones simultaneously without inflicting the kind of damage associated with microelectrodes. It is worth noting, however, that this quasi-crystalline regularity of the guinea-pig myenteric plexus is not shared by other animal species and that, even within the guinea-pig small intestine, some regional variation has been described (see, for example, Chapter 2 of Furness and Costa, 1987). However, when muscle contraction is inhibited and, therefore, no tension is present to distort the ganglionic scaffolding, the recurring pattern of the myenteric network along the small intestine becomes so obvious that it cannot be ignored.

The strikingly different anatomical organization of submucous and myenteric plexuses may reflect the functional requirements of the respective motoneurone–effector interactions. Submucosal motoneurones are, for the most part, involved in secretion, which is locally isotropic in the absence of myenteric inputs (Hubel et al., 1991; Moore and Vanner, 1998, 2000; Song et al., 1992). Myenteric motoneurones, by contrast, are primarily responsible for intestinal motility and, therefore, must be integrated into inherently anisotropic circuits designed to generate contraction orally and relaxation aborally (‘the law of the intestine’; Bayliss and Starling, 1899). Since both plexuses exhibit strong nicotinic innervation, and immunocytochemical data suggest that the same nAChR-subtypes are present in each (Obaid et al., 2001), we record from both plexuses at different spatial scales to elucidate features of the nicotinic circuits.

In 1998, auto-antibodies to neuronal α3-nAChRs were detected in patients with autonomic neuropathies that included symptoms such as gut dismotility (Vernino et al., 1998). Also, immunization of rabbits with α3-subunit protein has provided an animal model for this disorder (Vernino et al., 2003). The role played by α3-nAChRs in these syndromes is fully consistent with the ubiquitous expression of these nAChRs in the guinea-pig ENS, as shown by the immunocytochemistry and pharmacological experiments reported here. A similar antigenic behaviour is seen in myasthenia gravis, an autoimmune disorder of neuromuscular transmission (Lindstrom, 2000b; Lindstrom et al., 1976) that can be reproduced in mammals by immunization with the α1-nAChRs of skeletal muscle and fish electric organs. These examples illustrate the connection between nAChRs and autoimmunity. Considering that smoking has profound, but opposite, effects in two other autoimmune disorders, Crohn’s disease and ulcerative colitis (Green et al., 1997a,b; Osborne and Stansby, 1994; Zins et al., 1997), a better understanding of immune responses to nAChRs, and of the role(s) played by these receptors in gastrointestinal function, may help to elucidate the complex relationships between nicotine and inflammatory bowel disease (Osborne and Stansby, 1994). Towards that goal, we have begun to clarify some of the distinct contributions of individual nAChR-subtypes to the behaviour of enteric networks by imaging evoked electrical activity with voltage-sensitive dyes and applying specific antagonists to various nAChR-subtypes.

Materials and methods

Characterization of guinea-pig nAChRs using radioimmunoassays (RIAs)

Extracts of guinea-pig nAChRs

Frozen brains or frozen small intestines (cleared of their contents), previously excised from 150–200 g Hartley guinea pigs [*Cavia porcellus* (L.); Charles River Laboratories, Wilmington, MA, USA] that had been anesthetized by halothane inhalation and decapitated in accordance with institutional guidelines, were immersed in buffer A (50 mmol l^{-1} Na_2HPO_4–NaH_2PO_4, pH 7.5, 50 mmol l^{-1} NaCl, 5 mmol l^{-1} EDTA, 5 mmol l^{-1} EGTA, 5 mmol l^{-1} benzamidine, 15 mmol l^{-1} iodoacetamide and 2 mmol l^{-1} phenylmethylsulfonyl fluoride) at room temperature (RT) and mechanically disrupted using a Polytron homogenizer (Brinkman/Kinematica, Westbury, NY, USA). Cell membranes were collected by centrifugation (302 000 ***g***, 45 min), and the membrane pellets were subjected to detergent extraction by suspension in buffer B [buffer A that contained 2% Triton X-100 (Sigma Chemical Co., St Louis, MO, USA)] in an approximate ratio of 4:1 (v/w).

Liquid-phase RIAs

For immunoprecipitation assays, extracts of brain or gut were incubated with excess monoclonal antibody (mAb) in the presence of 2 nmol l^{-1} [^{3}H]epibatidine for 12 h at 4°C. mAb 210 (Lindstrom et al., 1996; Tzartos et al., 1987; Wang et al., 1996) was used to test for the presence of α3/α5-nAChRs; mAb 313 (Whiting et al., 1991) was used to test for α3-

nAChRs; mAb 299 (Whiting and Lindstrom, 1988) was used to test for α4-nAChRs; mAb 295 (Whiting and Lindstrom, 1988) was used to test for β2-nAChRs; and mAb 337 (Nelson et al., 2001) was used to test for β4-nAChRs. Excess goat anti-rat immunoglobulin G (IgG) (or goat anti-mouse in the case of mAb 337) was then added to precipitate mAb-bound nAChRs, for 2 h at 4°C. Subsequently, the mixtures were diluted 1:10 with phosphate-buffered saline (PBS) that contained 0.5% Triton X-100 (PBS/Triton) and centrifuged (12 385 ***g***, 10 min). The pellets were washed two more times with the PBS/Triton and then suspended in 2.5% sodium dodecyl sulphate (SDS) with 5% β-mercaptoethanol. The amount of [^{3}H]epibatidine bound was determined by liquid scintillation counting. Background was determined by parallel assays that contained normal rat (or mouse, when appropriate; see Table 1) serum instead of the mAb used for testing. To identify α7-nAChRs, we utilized the same protocol with mAb 306 (Schoepfer et al., 1990) and substituted ^{125}I-conjugated α-bungarotoxin ([^{125}I]αBgT) for [^{3}H]epibatidine.

Tissue preparation for physiological experiments

The submucous and myenteric plexus preparations were isolated by sequential dissection from the small intestine of 150–200 g Hartley guinea pigs that had been anesthetized by halothane inhalation and decapitated (in accordance with institutional guidelines). The dissection of the submucous plexus was performed as originally described by Hirst and McKirdy (1975), while the small intestine was bathed in a modified M199 medium (M3769; Sigma) supplemented with 5 mmol l^{-1} $NaHCO_3$, 20 mmol l^{-1} Hepes and 2 mmol l^{-1} glutamine. Before dissection of the myenteric plexus (which was achieved by pulling away the circular muscle fibres), 1–5 μmol l^{-1} nifedipine was added to the M199 to prevent smooth muscle contraction. (L-type calcium channel blockers neither block synaptic transmission nor alter vasodilator responses in the ENS; Bornstein et al., 1991; Moore and Vanner, 2000; Reed and Vanner, 2003; Vanner, 2000.) Once added, the presence of nifedipine was maintained throughout the experiment. To reduce background fluorescence from dye bound to residual smooth muscle and connective tissue, both isolated plexuses were incubated for 1 h at room temperature in their respective M199 media containing 50 U ml^{-1} collagenase VII (Sigma) and 0.5 mg ml^{-1} protease IX (Sigma). After this treatment, the preparations were washed with, and maintained in, their respective media, plus 10% foetal horse serum (FHS; Pel-Freez Biologicals, Rogers, AR, USA) and antibiotics (penicillin, 100 U ml^{-1}; streptomycin, 100 mg ml^{-1}; Gibco, Invitrogen Corp., Grand Island, NY, USA) for 24–48 h at RT. All preparations were then kept in a chamber equilibrated with 95% O_2/5% CO_2 until used. Since the functional studies require intact ganglionic networks, and the dissection procedures often jeopardize their integrity, we dissected double the number of submucous and myenteric segments needed for physiology. Careful inspection of the preparations under dark field, prior to each experiment, allowed us to select the most suitable segments for network studies. The remaining segments were typically used for immunocytochemistry. To control for possible changes in chemical phenotype of enteric neurones during the 24–48 h incubations, segments of both enteric plexuses, obtained from adjacent regions of the same preparation, were used for immunocytochemical identification of individual nAChR-subunits, either immediately after dissection or following the 24–48 h incubation (see below). Both groups of samples exhibited identical expression of nAChR-subtypes and comparable immunofluorescence intensity, confirming that no appreciable alteration of nAChR expression had taken place during the course of our experiments (see also Song et al., 1997a).

Tissue preparation for immunocytochemical assays

Immediately after the enzyme treatment, or following the 24–48 h incubation in the appropriately modified M199, the submucous and myenteric preparations (see previous section) were washed with PBS to eliminate any residual FHS and fixed in 10% buffered formalin (Fisher Scientific, Pittsburgh, PA, USA), for 24 h at 4°C. Obviously, this rather elaborate tissue preparation, while crucial for functional studies using voltage-sensitive dyes, is not essential for the immunocytochemical assays reported here, since, as reported in the previous section, similar results have been obtained with preparations fixed immediately after dissection.

Immunocytochemical identification of individual nAChR-subunits

Immunofluorescence experiments were performed on

Table 1. *Antibodies to nAChR-subunits used in this study*

mAb	Specificity	Immunogen	Species immunized	Original description
mAb 35	α1, α3, α5	Electric organ nAChR	Rat	Tzartos et al. (1981)
mAb 210	α1, α3, α5	Mammalian muscle nAChR	Rat	Tzartos et al. (1987)
mAb 313	α3	Bacterially expressed chicken α3	Rat	Whiting et al. (1991)
mAb 299	α4	Rat brain nAChR	Rat	Whiting and Lindstrom (1988)
mAb 306	α7	Rat and chicken α7-nAChR	Mouse	Schoepfer et al. (1990)
mAb 295	β2	Rat α4β2-nAChR	Rat	Whiting and Lindstrom (1988)
mAb 337	β4	Bacterially expressed human β4-cytoplasmic domain	Mouse	Nelson et al. (2001)

segments of submucous or myenteric preparations fixed as whole mounts. In experiments in which only one mAb was employed (e.g. those summarized in Figs 1, 2A,B), non-specific binding was reduced by exposure to 4% (v/v) normal goat serum (Jackson ImmunoResearch Laboratories, West Grove, PA, USA) in PBS/NaN_3, with Triton X-100 (0.5%) for permeabilization, for 2 h at RT. The fixed preparations were then exposed for 24–48 h, at 4°C, to the mAb of choice. The mAbs (see Table 1) were diluted to a final IgG concentration of 7–35 nmol l^{-1} (assuming IgG M_r=150 000) in PBS/NaN_3 containing 4% normal goat serum (goat serum/PBS/NaN_3), with Triton X-100 (0.5%). Following the incubation with the mAb, the samples were washed (three times, 30 min each) with the serum solution and subsequently exposed to the secondary antibody. Affinity-purified secondary antibodies [goat anti-rat (GART), goat anti-mouse (GAMS) and goat anti-rabbit (GARB); all IgGs; conjugated with indocarbocyanine (Cy3), fluorescein isothiocyanate (FITC) or Texas Red (TR); all from Jackson ImmunoResearch Laboratories], were diluted 1:1000 in PBS/NaN_3 containing 4% normal goat serum, with the addition of 0.5% Triton X-100. In some experiments (e.g. Figs 3, 4), we used mAb 210 that had been directly labelled with Alexa 488 or Alexa 594 fluorescent dyes using protein-labelling kits (A-10235 and A-10239; Molecular Probes, Eugene, OR, USA). All the experiments were performed on fixed tissue and included an incubation of 24–48 h with the selected mAb. Shorter exposures with dye-conjugated mAbs on live tissue (not shown) produced similar results. In addition, Alexa 594-conjugated αBgT (B-13423; Molecular Probes) was used in conjunction with mAb 306 to assist in the localization of α7-nAChR (Fig. 2). The Alexa 594-conjugated αBgT (250 nmol l^{-1}) as well as the Alexa 488- or Alexa 594-conjugated mAb 210 (7 nmol l^{-1}) were applied for 24 h, immediately following the enzyme treatment, while the live samples were bathed in M199 containing 10% FHS and antibiotics. Following exposure to the Alexa 594-conjugated αBgT or Alexa 488- or Alexa 594-conjugated mAb 210, the preparations were fixed as usual.

When double-staining was required, as in the experiments described in Figs 3, 4, we employed primary antibodies raised in the same or different species, but with one of them (mAb 210) conjugated with a fluorescent dye. In these examples, the first primary antibody had been raised in mouse (mAb 306; Fig. 3) or rat (mAb 295; Fig. 4) while the second primary antibody (mAb 210) had been raised in rat. The double-labelling protocol involved the following steps: (1) pre-incubation with 4% goat serum in PBS/NaN_3 containing 0.5% Triton X-100 to saturate non-specific binding sites for goat-IgGs; (2) incubation with the first primary antibody [mAb 306 (Fig. 3) or mAb 295 (Fig. 4) in 4% goat serum/PBS/NaN_3 containing 0.5% Triton X-100]; (3) washing of the first primary antibody; (4) incubation with the secondary antibody, which consisted of FITC-conjugated GAMS (Fig. 3) or TR-conjugated GART (Fig. 4) in 4% goat serum/PBS/NaN_3/Triton X-100; (5) washing of the secondary antibody; (6) incubation with 4% rat serum in PBS/NaN_3/Triton X-100 for 2 h at RT to saturate non-specific rat-IgG binding sites prior to the addition of mAb 210; (7) incubation with Alexa 594- (Fig. 3) or Alexa 488-conjugated mAb 210 (Fig. 4) for 24–48 h at 4°C; (8) washing of Alexa-conjugated mAb 210.

The antibody-labelled tissue segments were mounted in the anti-fading agent Pro-Long (Molecular Probes), covered with a cover slip and kept in the dark at 4°C until examined. Every experiment included parallel controls, in which whole mounts were incubated with PBS/NaN_3 containing the appropriate 4% normal serum in the absence of primary antibodies and subsequently stained with the corresponding secondary antibody. Double-staining experiments, such as those described above, included controls in which only the unlabelled primary antibody was omitted.

Immunofluorescence was visualized using a Leica TCS-NT laser scanning confocal microscope (Leica Microsystems Heidelberg GmbH, Mannheim, Germany), equipped with either a 40× (Leica, 1.25 N.A. oil PL APO) or a 100× (Leica UV, 1.4 N.A. oil PL APO) objective. Usually, 16–32 optical sections were taken at 0.486 μm intervals. Images acquired at 1024×1024 pixel resolution were processed using Adobe Photoshop 7.0 (Adobe Systems, Mountain View, CA, USA).

Multiple site optical recording of transmembrane voltage

Optical apparatus

The system for MSORTV comprised a NeuroCCD-SM camera (RedShirtImaging, Fairfield, CT, USA) and a relay lens (Diagnostic Instruments, Inc., Sterling Heights, MI, USA) mounted on the side port (converted to 100%/0% with the substitution of a first surface mirror for the manufacturer-supplied beam splitter) of an IM-35 inverted microscope (Carl Zeiss, Oberkochen, Germany). The microscope was arranged to move independently of a stage that was rigidly fixed to the top of a vibration isolation table (MinusK Technology, Inc., Inglewood, CA, USA), and the entire measuring system was mounted on a large motorized, digitally encoded and computer-controlled *X–Y* positioner (Motion Master 2000 Controller, Newport, Irvine, CA, USA). Epi-illumination was provided by a 150 W xenon short arc lamp (Osram, Munich, Germany) powered by an ultra-low-ripple, feedback-stabilized power supply (Opti-Quip, Highland Mills, NY, USA). The incident light was made quasi-monochromatic using a heat filter (KG-1; Schott Optical Glass, Duryea, PA, USA), a high-Q interference filter (530±25 nm; Chroma, Inc., Rockingham, VT, USA) and a dichroic mirror (560 nm); its intensity was adjusted using neutral density filters. Fluorescence emission was separated using an OG570 barrier (long-pass) filter (Schott Optical Glass). Trans-illumination, for bright-field or phase-contrast viewing of the preparation, was provided by a 12 V, 100 W tungsten–halogen lamp powered by an ATE 75-15 power supply (Kepco, Flushing, NY, USA). The experimental preparation was pinned onto a silicon inset and held flat against a #0 cover slip using a metal ring held in place by micro-clamps. The recording chamber was attached to the fixed stage, and a moveable front surface mirror permitted the projection of a real image of the preparation onto the NeuroCCD-SM

camera mounted at the side port. The electronic design and performance characteristics of the NeuroCCD-SM MSORTV system have been described in detail (Obaid et al., 2004). Briefly, it is a cooled, low-resolution, precision high-speed camera that uses the back-thinned, back-illuminated Marconi CCD39-01 chip (80×80 pixels). Digitization is 14 bit, and the full frame rate is 2 kHz (3×3 binning permits 5 kHz). The camera has the advantage of extremely low read noise (23 electrons at 2 kHz; 9 electrons at 1 kHz, and 4 electrons at 125 Hz). In addition, the chip has a relatively large well depth (215 000 $\mathbf{e}^-$), permitting moderate light intensities at high frame rates.

As an integral part of the apparatus, a specially designed secondary beam splitter on the trinocular tube of the microscope can be moved into and out of the light path. This device, combined with a projection lens, relays an image of the preparation onto a second, high-resolution, CCD camera (Hamamatsu Photonics, KK, Hamamatsu City, Japan) connected to a frame grabber (DT3120K-1; Data Translation, Marlboro, MA, USA). In this way, a high-resolution image of the preparation can be superimposed on the display of millisecond time-resolved optical signals provided by the NeuroCCD-SM camera to yield an accurate map of the spatial origins of the MSORTV signals.

Spatial resolution

The high-speed camera has, effectively, 5500 pixels within the central region of the 80×80 pixel chip, resulting in a spatial resolution that corresponds to single pixels having 'receptive fields' ~2.5 μm on a side in the object plane when a 100× objective is employed. The camera software (NeuroPlex; RedShirtImaging) permits arbitrary binning (spatial averaging) of pixels, allowing summation of the output of all the pixels that capture fluorescence emission from a single neurone or an entire ganglion.

Optical recording

The preparation was mounted in the recording chamber attached to the fixed stage of the inverted microscope. The tissue was stained for 30 min with 50 μg ml^{-1} of di-4-ANEPPDHQ (also known as JPW5029) (Obaid et al., 2004) in modified M199. Since the stock solution for the dye was made in ethanol, the final ethanol concentration in the staining solution was 0.25% v/v. The dye solution was washed out with modified M199 containing 2.5 U ml^{-1} glucose oxidase (Sigma) and 875 U ml^{-1} catalase (Sigma), and the experiments were carried out in that medium at RT (22–25°C). Optical recordings of electrical activity with single-cell resolution were obtained from the *in vitro* submucous- and myenteric-plexus preparations using either a 40× (DApo 40 UV 1.3. N.A. oil; Olympus Optical Co., Ltd, Tokyo, Japan) or a 100× (DPlanApo 100 UV 1.3 N.A. oil; Olympus Optical Co., Ltd) objective. Electrical activity was evoked by means of brief shocks (20 V, 0.5 ms) delivered by a 25 μm Teflon™-coated platinum (Pt) wire with its tip bared (FHS, Brunswick, ME, USA). It should be noted that the techniques employed in these experiments are not appropriate for quantitative taxonomy of nAChR-subtypes. Because stimulation typically is limited to 1–2 connectives per ganglion, the number of nAChRs of a particular subtype that contribute to a given evoked synaptic response represents a *lower bound* on the total number of receptors present in individual neurones. In addition, the contribution of a given nAChR depends upon its pre-, post- or peri-synaptic location and is modulated by the activity of neighbouring non-nicotinic receptors. Thus, the emphasis of the experiments described here is not so much on quantitation as on the identification of the role of individual nAChR-subtypes in circuit behaviour. Problems of phototoxicity, dye bleaching and dye internalization associated with di-4-ANEPPDHQ (JPW5029), together with their solutions, have been described elsewhere (Obaid et al., 2004).

Stability of optical recordings as a pre-condition for pharmacological experiments in submucous and myenteric plexuses

We performed 'sham' experiments, on both submucous and myenteric plexuses, in which we examined the effects of washing and of repeated periods of illumination on the size of the optical signals. While continuous superfusion (~10 ml at 1 ml min^{-1} for a 1 ml chamber) resulted in the loss of optical signal of up to 20%, gentle emptying and refilling of the chamber with a pipette never reduced the peak amplitude of the signal by more than 10%. Under different experimental protocols, constant perfusion may be practicable. Others (Neunlist et al., 1999; Schemann et al., 2002), using focal application (pressure injection) of the voltage-sensitive dye, have apparently been able to superfuse continuously without deterioration of the optical signals. However, bath application of the dye (see above) is more gentle and yields optical signals having noticeably better signal-to-noise ratio (cf. Obaid et al., 1999a, 2004). For this reason, following staining, we always changed solutions by pipette, and, when testing the effects of drugs, the experiments were designed so that the agents were added sequentially, without attempting to wash them out. At the same time, successive periods of illumination ($\leqslant$3 s) decreased the amplitude of the signals by 1–5%, primarily by bleaching. By contrast, all the pharmacological effects reported here substantially exceeded these limits. These sham experiments confirmed the expected advantages of sensitive high-speed optical recordings. Reduced light levels decreased photodynamic damage, allowed repetitive trials with good signal-to-noise ratio and minimized deterioration of the preparation (Obaid et al., 2004). In every optical experiment, two identical control recordings were required before any drugs were applied. Of 38 experiments (28 using submucous plexus and 10 using myenteric plexus), only seven (all submucous) failed to satisfy this criterion and were discarded.

Demonstration of the functional relevance of different nAChR-subtypes by MSORTV and pharmacology

By imaging electrical activity with voltage-sensitive dyes and a high-speed (1000 frames s^{-1}) CCD camera and applying

antagonists specific for various nAChR-subtypes, we could show that several subtypes play a functional role in both enteric plexuses. Electrical activity was elicited by low-frequency stimulation (2–3 pulses, 1–2 Hz, 0.5 ms, with the exception of Fig. 11, in which the duration of the pulses was 3 ms) applied through a monopolar electrode (Pt wire, 25 μm tip) positioned on a neighbouring ganglion or an inter-ganglionic connective. The intensity of the stimulus was set below action potential threshold, and the time course of the optical signal exhibited the characteristic synaptic duration (Obaid et al., 2004). To isolate the nicotinic component of the cholinergic response, all the experiments were performed in the presence of atropine (500 nmol l^{-1}) to block muscarinic receptor activity. In addition, all the experiments using myenteric plexus included nifedipine (1–5 μmol l^{-1}) to prevent muscle contraction. The specific antagonists employed for the different nAChR-subtypes were methyllycaconitine (MLA; 50 nmol l^{-1}; Alkondon et al., 1992) for α7, α-conotoxin (α-Ctx) MII (20–200 nmol l^{-1}; Cartier et al., 1996) for α3β2, and α-CTx AuIB (10–20 μmol l^{-1}; Luo et al., 1998) for α3β4. Mecamylamine (Mec; 50 or 100 μmol l^{-1}), a non-competitive antagonist of *all* neuronal nAChRs subtypes, was used to block any additional nAChRs still unidentified. To avoid depletion through non-specific interactions of the α-CTxs with the chamber walls, all the bathing solutions included 1% FHS.

Nicotinic reagents

α-CTx MII and α-CTx AuIB were generous gifts of Dr J. Michael McIntosh (University of Utah, Salt Lake City, UT, USA). Nicotine, MLA and Mec were purchased from Sigma.

Results

Functional equivalence of guinea-pig nAChRs to those of other species, and specificity of the mAbs used in this study

Nicotinic transmission in the ENS is widely recognized, but the types and numbers of functional nAChR-subtypes in enteric connectivity remains unclear. Immunocytochemical studies using antibodies against neuronal α3-, α4-, α3/α5-, β2-, β4- and α7-subunits (Table 1) suggest that all these subunits, except α4, are present in the guinea-pig intestine (Kirchgessner and Liu, 1998; Obaid et al., 1999a,b; Obaid and Lindstrom, 2000). However, since guinea-pig nAChRs have not yet been cloned, the specificity of our mAbs and the functional equivalence of guinea-pig nAChRs to those of other species cannot be taken for granted. To address the issue of antibody recognition across species, we performed radioimmunoassays. Membrane fractions from brain or intestine of guinea pig were detergent-solubilized, centrifuged, and the supernatants used for liquid-phase binding assays. [^{125}I]αBgT was used with mAb 306 to identify α7, and [^{3}H]epibatidine was used with all the other mAbs – 313 for α3, 210 for α3/α5, 299 for α4, 295 for β2, and 337 for β4 – to identify heteromeric nAChRs. Our results (Obaid et al., 2001) are summarized in Table 2.

Table 2. *Relative distribution of nAChR-subunits in brain and small intestine extracts, as determined by liquid-phase RIAs*

		[nAChR] (pmol kg^{-1} wet tissue)*	
mAb	Specificity	Brain	Small intestine
mAb 210	α3, α5	177±7	140±30
mAb 313	α3	73±23	40±7
mAb 299	α4	254±53	5±3.6
mAb 306	α7	730±80	41±7
mAb 295	β2	775±35	66±6
mAb 337	β4	13±1	1±0.2

*Expressed as either [^{3}H]epibatidine binding sites for α3-nAChRs ± S.D. (N=3) or [^{125}I]αBgT binding sites for α7-nAChRs ± S.D. (N=3).

Localization of nAChR-subtypes in whole mounts of submucous and myenteric plexuses

Identification and localization of α3/α5-containing nAChRs

We have already shown (Obaid et al., 1999a) the surface binding (in fixed, non-permeabilized tissue) of mAb 210 and mAb 35 (Tzartos et al., 1981), two mAbs that recognize different epitopes within the main immunogenic region (MIR) of α1-nAChRs of muscle and cross-react with neuronal α3- and α5-subunits of the nAChR (Conroy and Berg, 1995; Wang et al., 1996, 1998). Surface immunoreactivity was observed widely on neuronal plasma membrane, revealing regions with a high density of nAChRs. We have also confirmed (data not shown) that the surface binding of mAb 210 to live tissue can be prevented by a 30 min pre-incubation of the enteric plexuses with a saturating concentration of mAb 35.

Fig. 1 compares the binding of mAb 210, which recognizes α3- and α5-subunits of the nAChR, to that of mAb 313, which selectively recognizes an intracellular epitope of the α3-subunit. The striking similarity in the patterns of immunoreactivity between both mAbs in permeabilized submucosal ganglia indicates that, at least in the submucous plexus, α3 is the most prevalent subunit in heteromeric nAChRs. Despite the near ubiquity of α3/α5 immunoreactivity (which, based on the data from Fig. 1 could be attributed mostly, if not completely, to α3), a few cells, positioned near connectives, were not labelled by these mAbs. These cells proved, very often, to be immunoreactive for substance P, which is an intracellular marker for sensory neurones (Bornstein and Furness, 1988; Kirchgessner and Liu, 1998; Obaid et al., 2001).

Identification and localization of α7-nAChRs

Fig. 2 illustrates the distribution of homomeric (Chen and Patrick, 1997; Drisdel and Green, 2000) α7-nAChRs in submucosal ganglia. Fig. 2A shows a confocal image after labelling with mAb 306, which recognizes both native and denatured chick α7-nAChRs (Dominguez del Toro et al., 1994; Schoepfer et al., 1990). Fig. 2B shows a negative control,

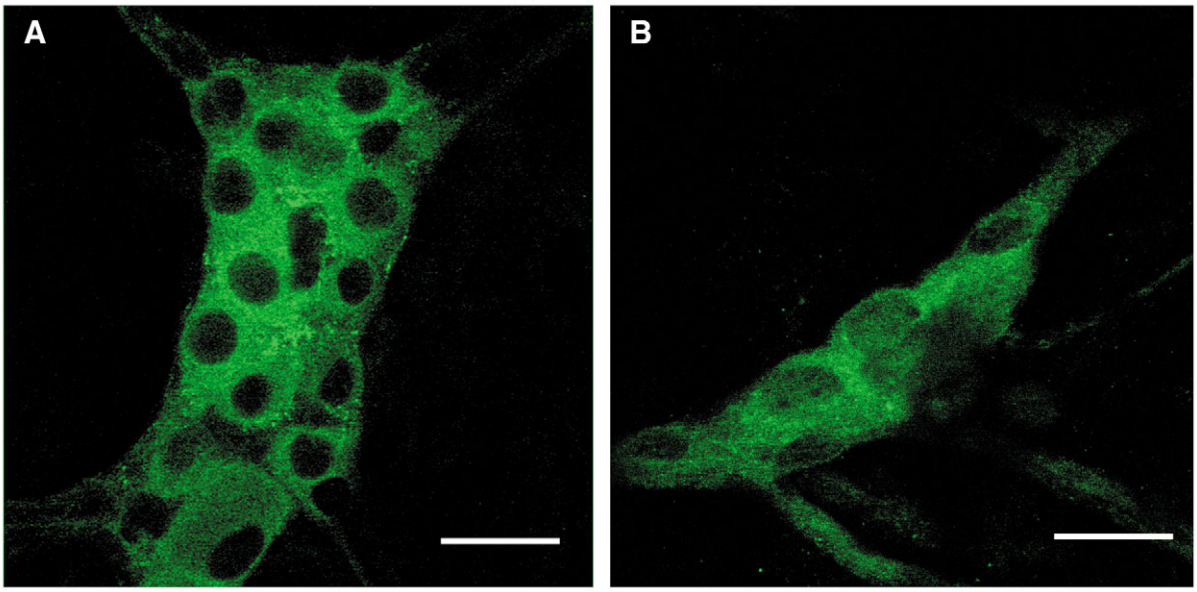

Fig. 1. mAb 313, which selectively recognizes α3-nAChRs, shows a pattern of immunoreactivity very similar to that exhibited by mAb 210 in permeabilized tissue. (A) Submucous ganglion stained with mAb 210 (17 nmol l^{-1}) and FITC-goat-anti-rat (1:1000). Scale bar, 25 μm. (B) Submucous ganglion stained with mAb 313 (35 nmol l^{-1}) and FITC-goat-anti-rat (1:1000). Scale bar, 20 μm. In both preparations, the tissue was permeabilized with 0.5% Triton X-100.

obtained from another segment of the same preparation used in Fig. 2A, in the absence of mAb 306. Since the epitope recognized by this mAb is intracellular (McLane et al., 1992), the tissue was permeabilized with 0.5% Triton X-100, giving mAb 306 access to both surface and intracellular α7-nAChRs.

It is obvious, from the image in Fig. 2A, that most submucosal neurones immunoreact with mAb 306. Because the specificity of mAb 306 has been questioned in other systems (Fabian-Fine et al., 2001), we have compared its binding distribution with that of αBgT. Fig. 2C shows a confocal image of a ganglion stained with Alexa 594-conjugated αBgT at a concentration of 250 nmol l^{-1}, the only concentration, in the range of 10–250 nmol l^{-1}, at which the αBgT-binding was detectable. In contrast with the binding of mAb 306, carried out on fixed and permeabilized tissue, the αBgT-binding was examined in live tissue, prior to fixation, in order to preserve the native conformation of the nAChR. A comparison of Fig. 2A and Fig. 2C underscores the identical patterns of labelling with mAb 306 and αBgT. These results suggest that α7-nAChRs are

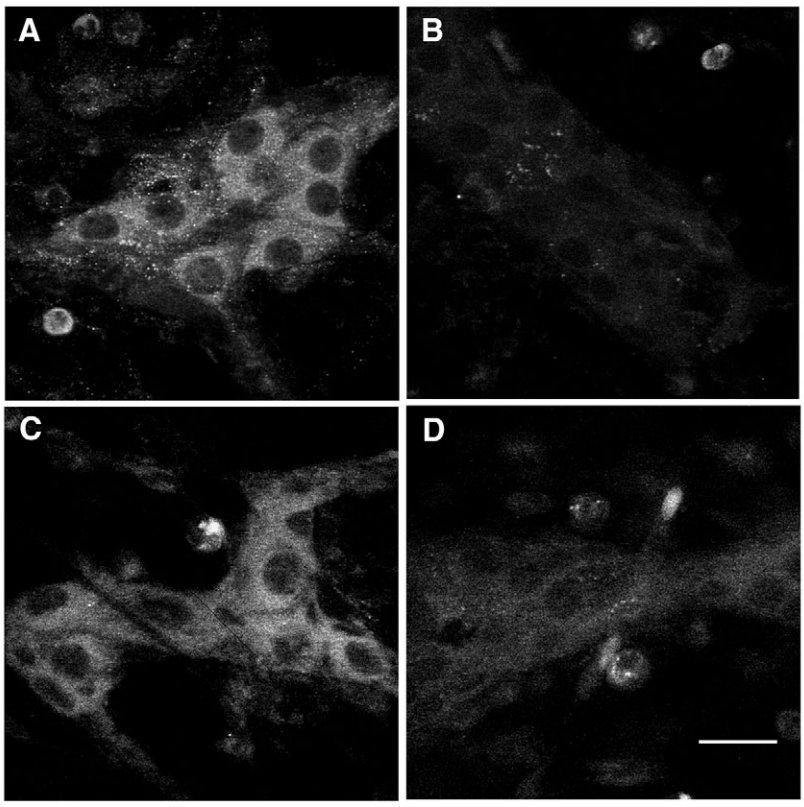

Fig. 2. The pattern of immunofluorescence obtained using mAb 306 mimics the distribution of αBgT-binding in submucosal ganglia, and the block of αBgT-binding by nicotine confirms that αBgT reacts specifically with enteric α7-nAChRs. (A) Submucosal ganglion stained with mAb 306 (17 nmol l^{-1}) and FITC-conjugated goat-anti-mouse. Fixed tissue permeabilized with Triton X-100 (0.5%). (B) Negative control for A, obtained from the same preparation in the absence of mAb 306. (C) Binding of Alexa 594-conjugated αBgT (250 nmol l^{-1}) to a live segment of submucosal plexus. (D) The binding of Alexa 594-conjugated αBgT was blocked by a 16 h co-incubation with 1 mmol l^{-1} nicotine. Scale bar, 25 μm.

primarily expressed on the surface of submucosal neurones and that, in contrast to heteromeric nAChRs, they tend not to cluster. Fig. 2D illustrates a section of submucosa that was prepared identically to that in Fig. 2C, except that the incubation with Alexa 594-conjugated αBgT was carried out in the presence of saturating (1 mmol l^{-1}) nicotine to compete for binding of αBgT. The lack of staining observed in Fig. 2D highlights the high specificity of binding of the Alexa 594-conjugated αBgT to α7-nAChRs. Altogether, the data presented in Fig. 2 confirm the ubiquitous expression of α7-nAChRs in submucosal neurones and validate mAb 306 as a powerful and highly specific probe for their recognition.

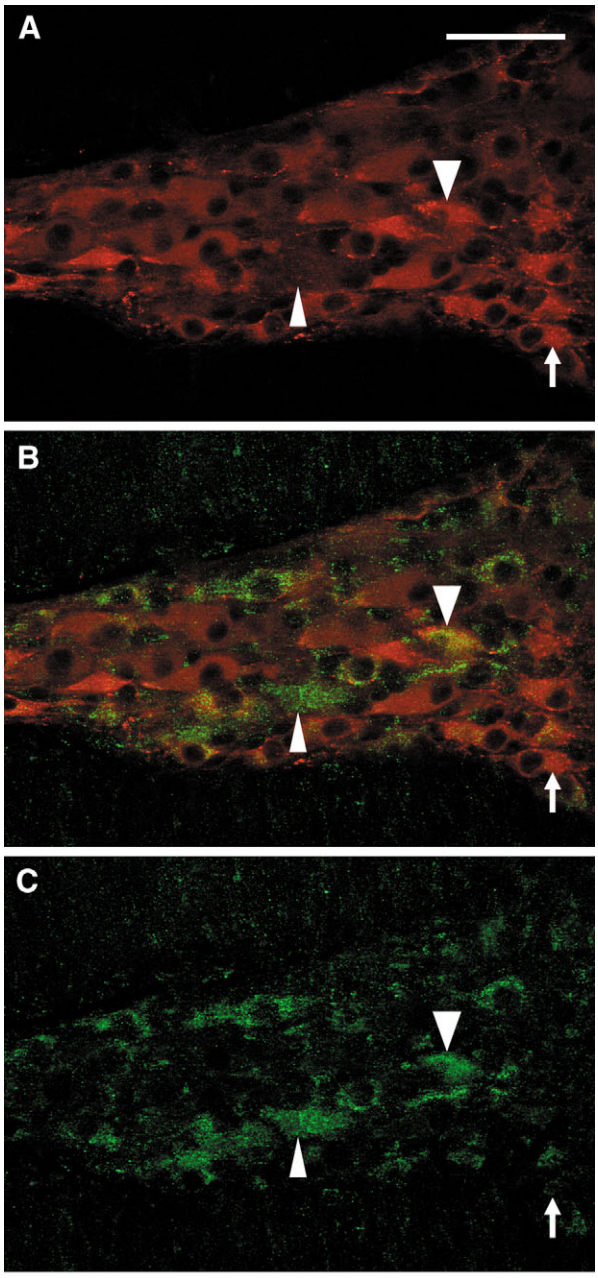

Fig. 3. α7-nAChRs are also present in myenteric plexus, but their distribution is not as ubiquitous as in the submucous plexus. (A,C) Red (Alexa 594-conjugated mAb 210, 7 nmol l^{-1}) and green (17 nmol l^{-1} mAb 306/FITC-conjugated goat-anti-mouse 1:1000) channels of a confocal micrograph taken from a myenteric ganglion double-stained for α3/α5- and α7-containing nAChRs. (B) Combined immunofluorescence from A and C. In A–C, the arrow points to a cell that expresses α3/α5- but not α7-nAChRs. The upward arrow head points to a cell that expresses α7- but not α3/α5-nAChRs. The downward arrow head points to a cell that expresses both types of nAChRs. Scale bar, 50 μm.

α7-nAChRs are also present in the myenteric plexus, but their distribution is not as ubiquitous as in the submucous plexus. Fig. 3, for example, shows the results of a double-staining experiment with mAb 210 and mAb 306. Analysis of these confocal images revealed that, in contrast to what we had observed in submucous plexus, α3/α5-nAChRs in myenteric plexus are much more abundant than α7-nAChRs.

Identification and localization of β2- and β4-containing nAChRs

β2-containing nAChRs are abundant in the enteric nervous system. In the submucous plexus (Fig. 4), as well as in the myenteric plexus (not shown), the pattern of β2-immunoreactivity is very similar to the pattern of immunoreactivity for α3/α5-nAChRs, suggesting that these subunits are structural partners in the same heteromeric nAChRs. However, the relative expression of the different subunits is quite variable, with some neurones expressing primarily one subunit over another. This can be readily seen in Fig. 4.

Functional studies using high-speed imaging and pharmacological probes

Heteromeric nAChRs

Figs 5–7 illustrate the effects of α-CTx MII (a specific antagonist for α3β2-nAChRs) and α-CTx AuIB (a specific antagonist for α3β4-nAChRs) on submucosal neurones. Fig. 5D shows optical recordings from the ganglion in Fig. 5A. Notice that the data are presented in two ways: (1) signals spatially averaged over the whole ganglion (top row of bars in Fig. 5D, labelled 'Ganglion', whose heights represent the amplitude of the voltage change averaged over the area of interest) and (2) signals spatially averaged over individual neurones ('Cells' numbered 1 to 11).

The optical signals from individual neurones in Fig. 5D, and changes in these signals induced by exposure to α-CTx MII, α-CTx AuIB and Mec, vary from cell to cell. This is not surprising, since these synaptic responses reflect both the density of individual nAChR-subtypes at the synaptic sites and the strengths of the incoming pre-synaptic inputs. Thus, any attempt to quantify the number of cells that exhibit a 'typical' response would be misleading. Instead, we have used the amplitude of the spatially averaged optical signal over the whole ganglion as a parameter that approximates the relative distribution of nAChRs activated in each experiment. An analysis of the kind of information that can be extracted from experiments such as that in Fig. 5 is given in Fig. 6.

Fig. 6A shows the optical responses, spatially averaged over the whole ganglion during the entire experiment, and Fig. 6B

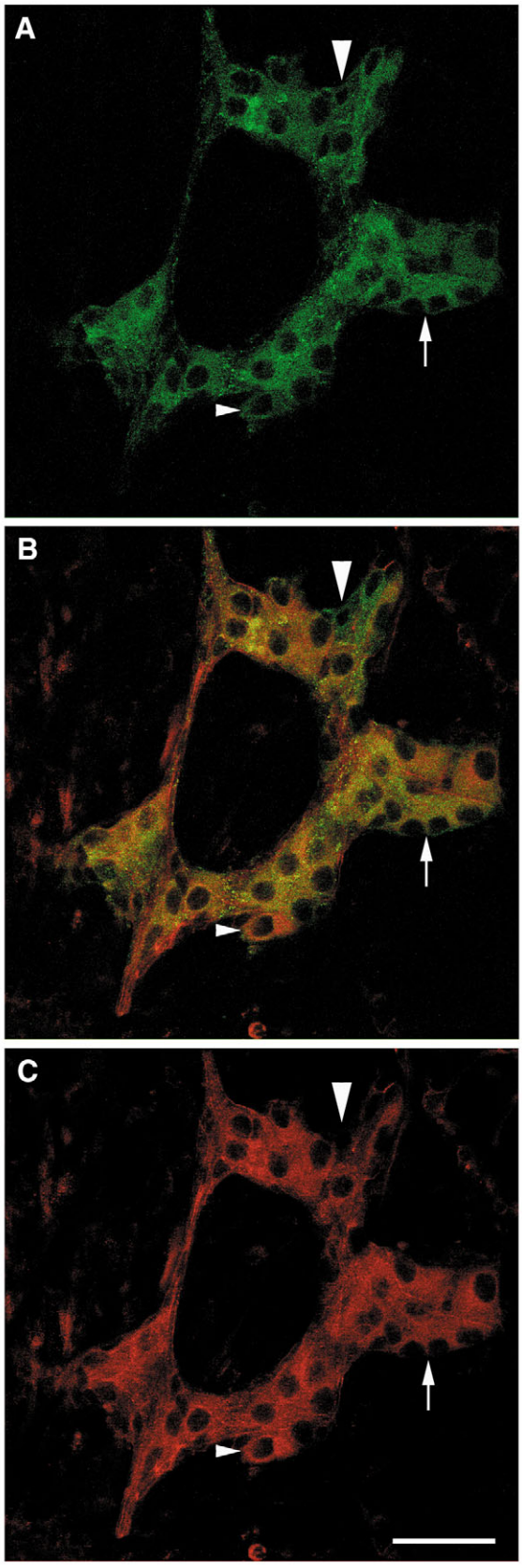

Fig. 4. The pattern of β2-immunoreactivity in the submucous plexus is very similar to the pattern of immunoreactivity for α3/α5-nAChRs, suggesting that these subunits are structural partners in the same heteromeric nAChRs. (A,C) Green (Alexa 488-conjugated mAb 210, 7 nmol l^{-1}) and red (33 nmol l^{-1} mAb 295/TR-conjugated goat-anti-rat 1:1000) channels from a confocal micrograph taken from a submucous ganglion double-stained for α3/α5- and β2-nAChRs. (B) Combined immunofluorescence from A and C. The upward arrow points to one of the multiple neurones that express α3/α5- as well as β2-nAChRs. The horizontal arrow head points to a cell that expresses predominantly β2-nAChRs. The vertical arrow head points to a cell that expresses mostly α3/α5-nAChRs. Scale bar, 50 μm.

depicts the percent inhibition resulting from each successive drug application. Note that the signal amplitudes plateau after each application of a new drug, demonstrating that the decreases in the magnitude of the responses reflect the antagonistic effect of each drug and are not due to gradual deterioration of the preparation. Fig. 6C illustrates distinct inhibitory effects of the different reagents on different cells.

Cell 2. Its evoked synaptic response was reduced by α-CTx MII, revealing the presence of α3β2- and/or α3β2β4-nAChRs. Further reduction by α-CTx AuIB indicates that this neurone also expressed α3β4-nAChRs as independent entities. Subsequent addition of Mec completely eliminated the response remaining after the block of all α3-containing nAChRs.

Cell 4. Its evoked synaptic response was also sensitive to α-CTx MII and α-CTx AuIB, but the addition of Mec did not eliminate all the residual response.

Cell 6. Its evoked synaptic response was less affected by the addition of the α-CTxs, and the large residual response in the presence of Mec suggests a greater role for non-nicotinic components.

Cell 8. Its pattern of evoked synaptic responses is intermediate between that of cells 4 and 6.

Cell 10. Unlike cells 2, 4, 6 and 8, this neurone's synaptic response was depressed by α-CTx MII but not by α-CTx AuIB. Mec produced a further reduction in the magnitude of the fast excitatory post-synaptic potential (epsp) but did not eliminate it.

Although similar stereotypical responses were identified in individual neurones from all 12 submucous ganglia examined, the 'ganglion' responses varied widely. In five experiments in which Mec was used to eliminate all residual nicotinic responses, the mean optical signals were reduced by 64.8±1.9% (S.E.M.) with respect to the control. Furthermore, the maximum inhibition (76%) was observed in the ganglion depicted in Figs 5 and 6, in which the stimulus reached the ganglion through two connectives simultaneously. This result implies that the nAChRs in a particular ganglion receive excitatory inputs from multiple ganglionic neighbours.

Fig. 7 shows a similar experiment, in which the order of application of the α-CTxs was reversed. The stimulating electrode, whose relative location (not to scale) is indicated schematically, was positioned on a neighbouring ganglion out of the field of view, so that the stimulus would reach the ganglion under study primarily through the connective adjacent to cell 15. Optical responses spatially averaged over the entire ganglion show a small effect of α-CTx AuIB, compared with

that of α-CTx MII. This result suggests that, in this particular ganglion, the incoming input activates a relatively small number of nAChRs containing the β4-subunit. Indeed, individually, cell 1 exhibits a pharmacological response that approaches that of the ganglion as a whole. However, in the majority of the cells (12 out of 15), the incoming stimulus activates different combinations of subunits. For example, the response of cell 11 includes the contribution of β4-containing nAChRs (in α3β4- and/or α3β2β4-subunit combinations) but not of pure α3β2-nAChRs. On the other hand, the fast epsp exhibited by cell 14 reflects the activation of α3β2-, α3β4 and $(\alpha3)_2(\beta2)_x(\beta4)_y$ but no other nAChR subtypes (e.g. α7).

Homomeric nAChRs

Fig. 8 illustrates the effect of blocking submucosal α7-nAChRs with MLA (at 50 nmol l^{-1}, a selective antagonist of these nAChRs) and underscores the substantial contribution of α7-nAChRs to the evoked signals. This is consistent with the ubiquitous distribution of these nAChRs in the submucous plexus, as revealed by immunocytochemistry (see Fig. 2). On an individual basis, most submucosal neurones were sensitive to MLA. Furthermore, the effect of α-CTx MII, following inhibition by MLA, was smaller than that observed when α-CTx MII was added alone. Indeed, following inhibition of α7-

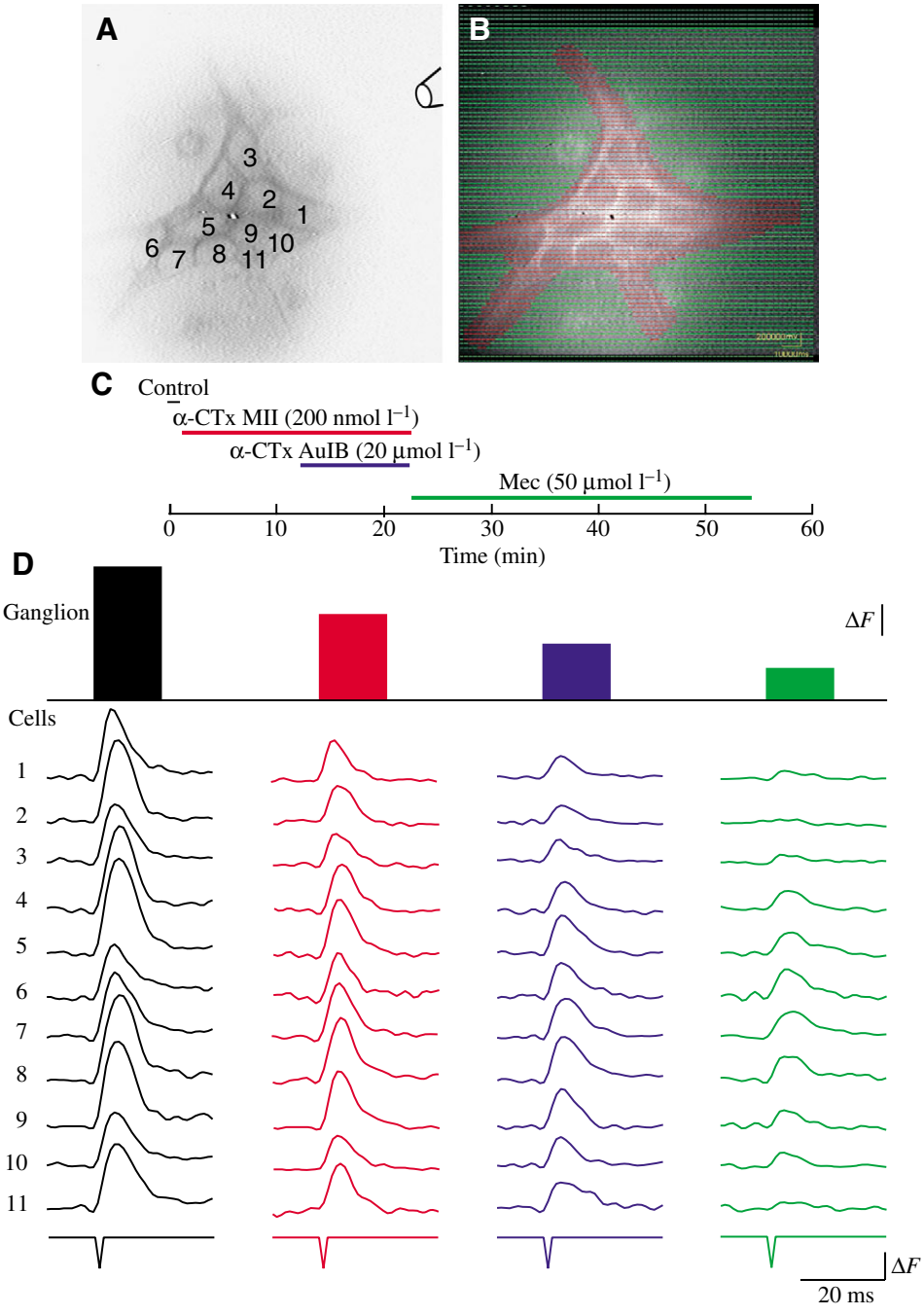

Fig. 5. High-speed camera recordings from submucous ganglia reveal the differential sensitivities of individual neurones to specific nAChR-antagonists. (A) High-resolution image of a submucous ganglion stained with the naphthylstyryl-pyridinium dye di-4-ANEPPDHQ (inverted grey scale), showing the individual neurones identified by numbers. The stimulation electrode, indicated schematically, was on an adjacent ganglion to the upper right, out of the field of view. (B) Pixel map of the NeuroCCD-SM camera depicting, in red, the pixels within the area of interest. (C) Experimental protocol. (D) High-speed optical recordings from the ganglion in A. Data are presented in two ways: signals spatially averaged over the whole ganglion [row of bars labelled 'Ganglion', whose heights represent the amplitude of the voltage change averaged over the area of interest (red pixels in B)] and signals spatially averaged over individual neurones ('Cells' numbered 1–11). The colours match the conditions illustrated in C and reflect the steady-state responses obtained during successive drug applications (see Fig. 6B,C). Since no absolute membrane potential calibration is possible in this type of experiment, the vertical axis in this and all subsequent optical recordings represents changes in fluorescence intensity in arbitrary units (Δ*F*). Illumination was reduced 21-fold by inserting neutral density filters in the light path; its duration was limited to 1.8 s per trial. Magnification, 100×. All traces were band-pass filtered between 6.6 and 200 Hz.

nAChRs, the response of some cells to α-CTx MII was negligible.

Functionally important nAChRs in the guinea-pig myenteric plexus

Fig. 9 illustrates the type of response observed in approximately half of the isolated myenteric plexus preparations challenged by the application of selective antagonists of β2- and β4-containing nAChRs. The results of this experiment are presented exclusively as the spatial average of all the optical responses over the entire ganglion and the bordering areas, to illustrate several points. First, the size and anatomical organization of myenteric ganglia differ from that of submucosal ganglia. In contrast to submucosal ganglia, whose neurones (~10–12 per ganglion, on average) are organized in a quasi-two-dimensional array, the myenteric ganglia (~150–200 neurones per ganglion) exhibit a pronounced three-dimensional structure. Therefore, fluorescence measurements of electrical activity in the myenteric plexus do not accurately reflect the activity of *all* the individual neurones in a particular ganglion. Instead, the principal contribution to the optical signals comes from those neurones that lie in the appropriate focal plane (Salzberg et al., 1977). Second, it is necessary to avoid the optical artefacts introduced by the slow waves of smooth muscle contraction. Despite the presence of atropine (500 nmol l^{-1}) and nifedipine (1–5 μmol l^{-1}) in the bathing solution, the longitudinal muscle layer that supports the plexus, as well as the residual circular muscle fibres that eluded dissection, can contract spontaneously, and gradually alter the shape of the ganglion under study and the registration of individual neurones with respect to the camera pixels. This behaviour, illustrated in the series of ganglionic images displayed in Fig. 11C, determines that the electrical activity of individual cells throughout the experiment can only be followed unequivocally in a relatively small number of neurones. Those neurones are selected taking into account several criteria such as constancy of shape, position with respect to immediate neighbours, and occasional fiducial marks such as bright spots within adjacent connectives and/or neuropile. By contrast, the optical signals averaged over the entire ganglion, while lacking single-cell resolution, reveal the overall effects of pharmacological interventions on synaptic circuits and facilitate the analysis of inter-ganglionic interactions. (Notice that the region of interest, indicated in Fig. 9B by the dark grey pixels, extends beyond the projected image of the ganglion. This is because we

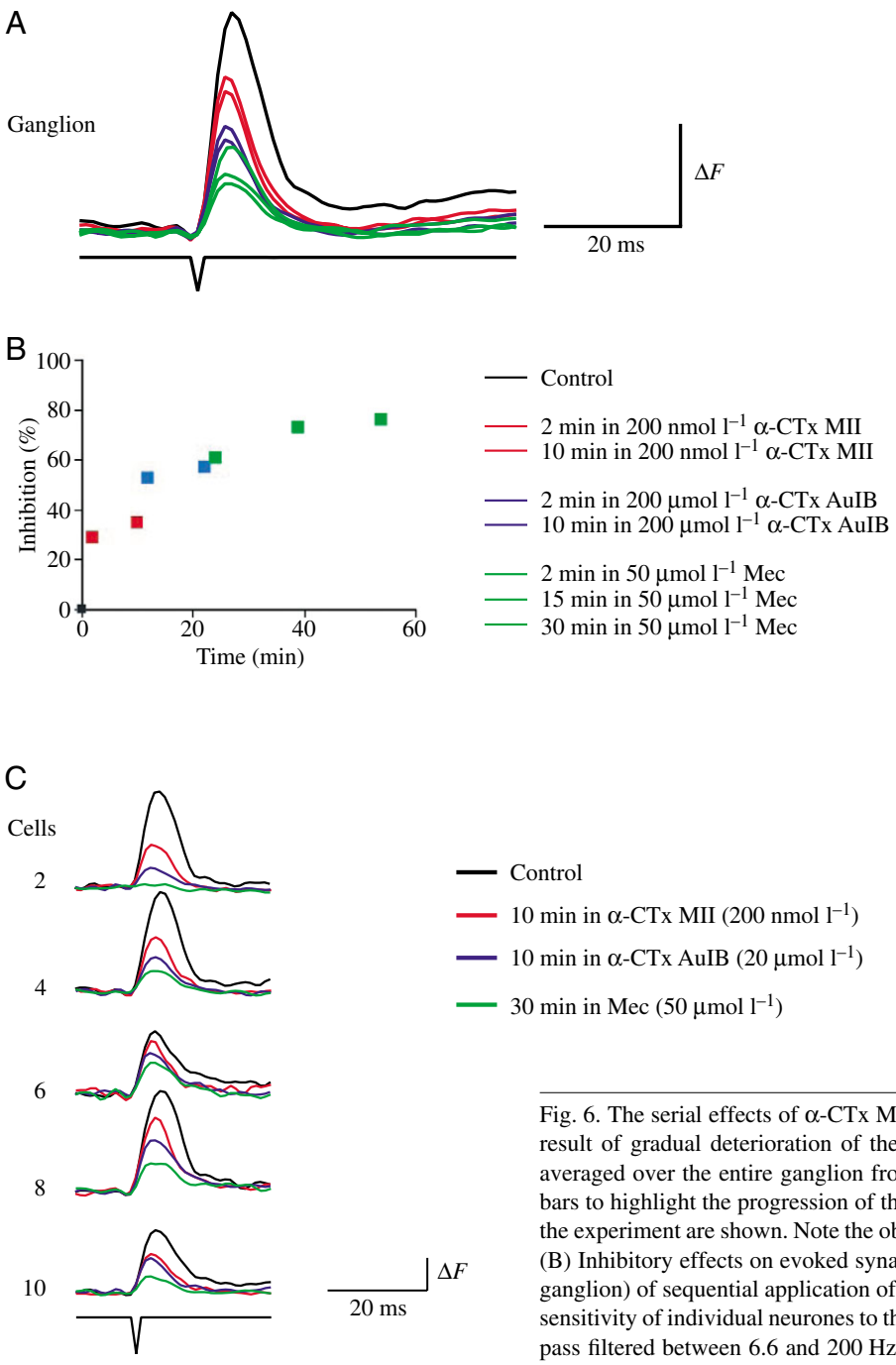

Fig. 6. The serial effects of α-CTx MII, α-CTx AuIB and Mec are additive and not the result of gradual deterioration of the preparation. (A) Actual optical traces, spatially averaged over the entire ganglion from the experiment in Fig. 5, are shown instead of bars to highlight the progression of the drug effects. Here, all the trials recorded during the experiment are shown. Note the obvious clustering of responses according to colour. (B) Inhibitory effects on evoked synaptic responses (spatially averaged over the whole ganglion) of sequential application of nAChR-antagonists. (C) Examples of differential sensitivity of individual neurones to these antagonists. As in Fig. 5, all traces were band-pass filtered between 6.6 and 200 Hz.

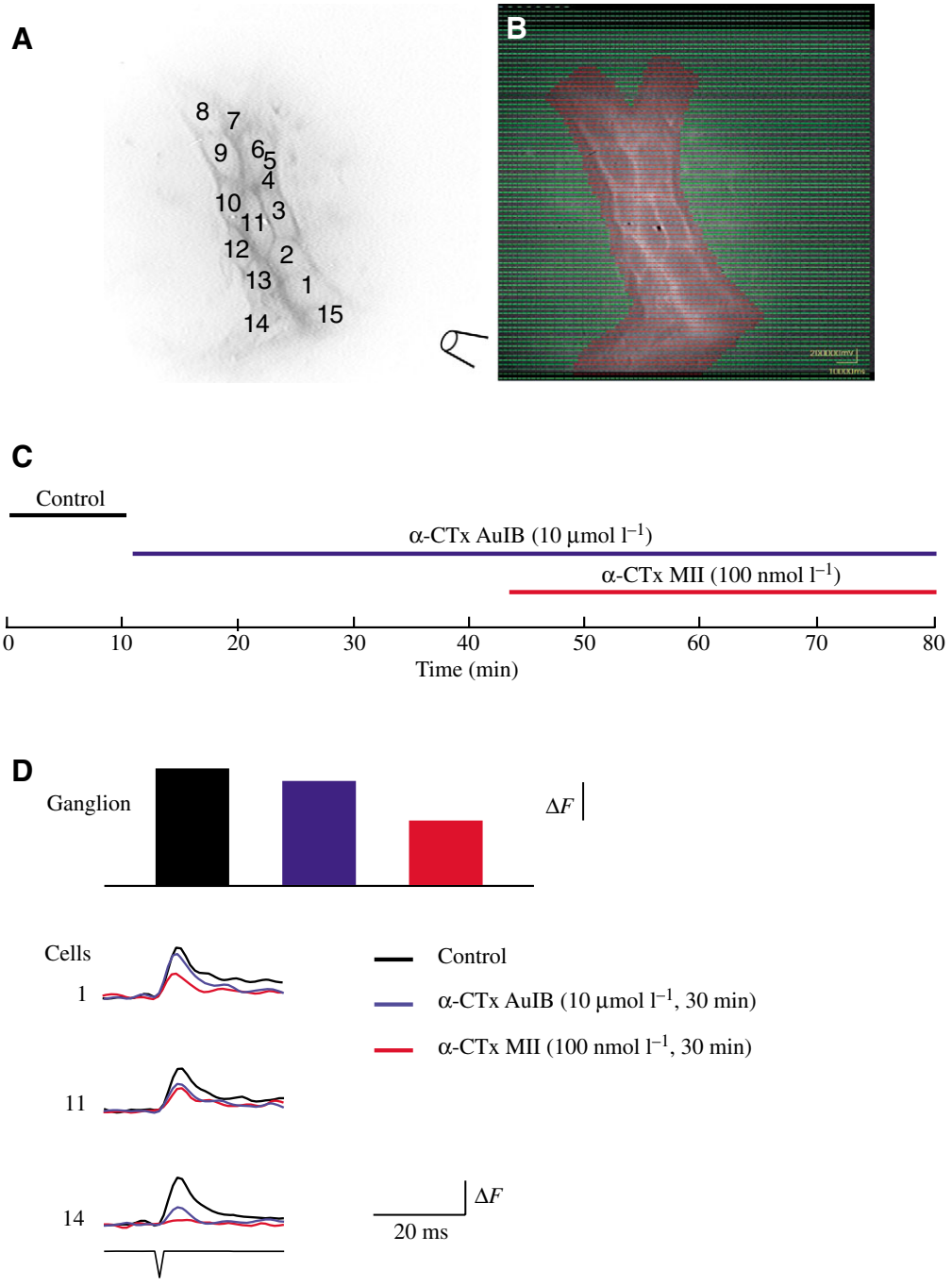

Fig. 7. The serial effects of α-CTx AuIB and α-CTx MII are also additive, suggesting that α3β2- and α3β4-nAChRs can exist as independent entities in submucosal neurones. (A) High-resolution image of a submucosal ganglion (inverted grey scale), showing the individual neurones identified by numbers. The position of the stimulation electrode is shown schematically. (B) Pixel map of the NeuroCCD-SM camera depicting, in red, the area of interest. (C) Experimental protocol. (D) Spatially averaged optical outputs from the red pixels in B (represented by bars whose heights indicate the amplitude of the voltage change under each experimental condition in the row labelled 'Ganglion') and from selected individual neurones ('Cells'). Magnification, 100×. 'Ganglion' signals were high-pass filtered at 6.6 Hz. 'Cell' traces were low-pass filtered at 200 Hz.

chose the region of interest to reflect the projection of *all* the configurations assumed by the ganglion throughout the experiment, not just the conformation at the instant that the photographic image was acquired.) The results presented in Fig. 9 mimicked the effects of α-CTx MII and α-CTx AuIB on submucous ganglia (illustrated above) and confirmed that α3β2- and α3β4-nAChRs can be found as independent entities in both enteric plexuses (albeit not on every neurone). This result, of course, does not necessarily exclude the occurrence of α3β2β4-nAChRs in the ENS.

In the remaining experiments (three of six preparations), performed under the same conditions, inhibition of nAChRs in the myenteric plexus resulted in paradoxical enhancements of the optical signals. The magnitude of the effect varied from neurone to neurone, and its occurrence could not be anticipated. To isolate the component of the evoked response mediated solely by heteromeric nAChRs, and to rule out a modulatory effect of α7-nAChRs, we applied MLA (50 nmol l^{-1}), prior to the addition of the α-CTxs. One of these experiments is shown in Fig. 10. To our surprise, examination of the optical signals from some cells (e.g. cell 2) revealed that MLA alone, prior to the application of the α-CTxs, *increased* the magnitude of their depolarizing responses, while the spatially averaged optical responses over the entire ganglion

decreased. Further addition of α-CTx MII enhanced the excitation throughout the ganglion. This paradoxical increase in the amplitude of the evoked response was also observed in the absence of MLA and could result from inhibition of α3β4-nAChRs by α-CTx AuIB as well (not shown). Mec, on the other hand, decreased the magnitude of the response. Note that many of the neuronal signals in Fig. 10 don't return to baseline. We may speculate that, since in myenteric-plexus experiments the electrode is at a considerable distance from the recording sites, summation of inputs from multiple axons, as well as reverberating activity, may explain the delay in the return to baseline.

All the experiments described thus far were carried out with the longitudinal axis of the enteric plexuses aligned with the *Y*-axis of the recording chamber. However, their oral–aboral polarity was not preserved. Considering the well-established longitudinal asymmetry of the myenteric circuits (Brookes et al., 1997; Song et al., 1996, 1997b, 1998), we suspected that circuit directionality might underlie the contrasting effects of nAChR antagonists in the myenteric plexus. We therefore resorted to dual stimulation. This protocol required two identical Pt-wire electrodes positioned orally and aborally with respect to the ganglion of interest. Two stimuli, one to each electrode, were delivered out of phase with one another, and this pulse sequence was repeated before and after the application of selective nAChR blockers. The order in which the stimuli were applied did not affect the size of the evoked responses. Fig. 11 illustrates one such experiment. In this example, a 25 min exposure to α-CTx MII inhibited the response evoked by electrode E_2 by approximately 40% over the whole ganglion, without affecting the response evoked by electrode E_1 in the same areas of interest. These effects are represented more definitively in the movies shown in Fig. 11G, where all the pixels are depicted individually. The panel on the right shows the responses to the stimuli from electrode 2 (E_2) under control conditions and after 25 min exposure to 100 nmol l^{-1} α-CTx MII. The decrease in the amplitude of the optical signals is apparent. By contrast, the corresponding responses to stimuli from electrode 1 (E_1), shown on the left, reveal little or no effect of the toxin. The different activity patterns evoked by E_1 and E_2 were observed in the four identified neurones, as well as over the entire ganglion, suggesting that most of the cells exhibited this behaviour. This ganglion was part of a network, all of whose ganglia were affected by the α-CTx MII. Therefore, the differential responses evoked by the two electrodes in the presence of the toxin probably resulted from the block of α3β2-containing nAChRs on the neurones (in neighbouring ganglia) that were pre-synaptic to those in the ganglion of interest.

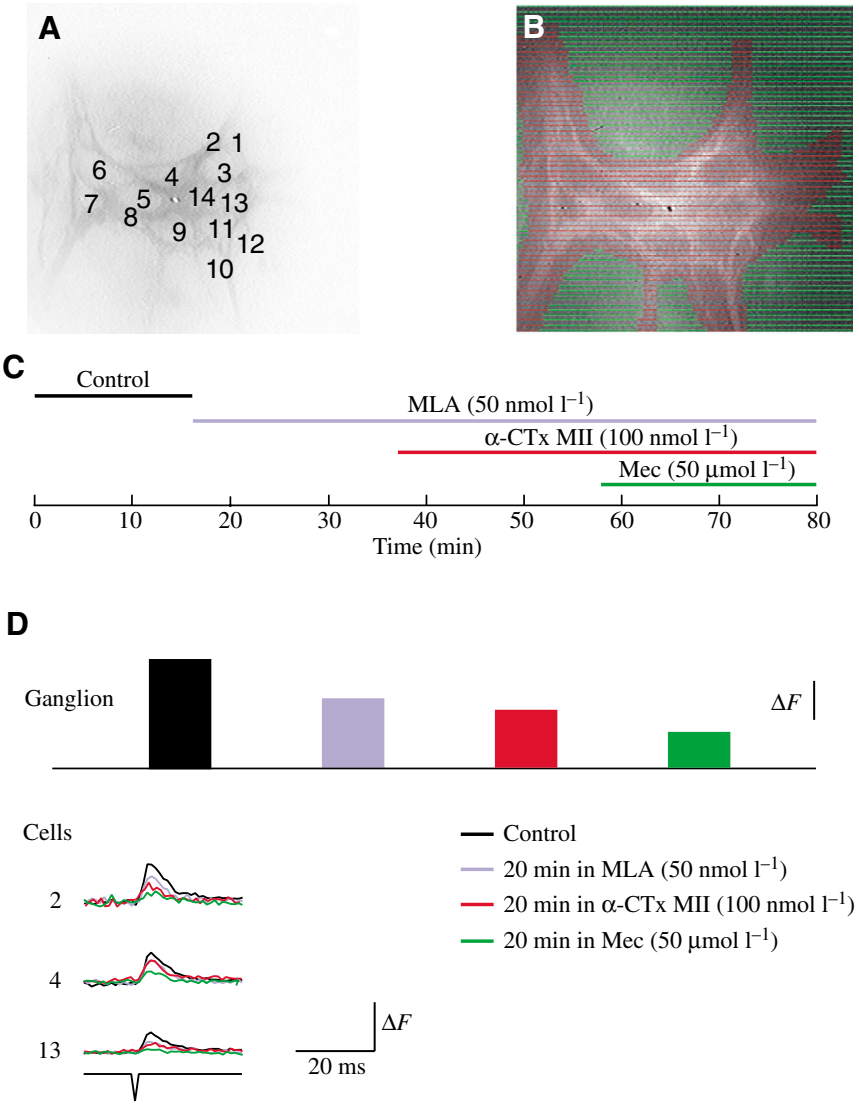

Fig. 8. α7-nAChRs contribute substantially to the evoked response in submucosal neurones. (A) High-resolution image of a submucosal ganglion (inverted grey scale), showing the individual neurones identified by numbers. The position of the stimulation electrode is shown schematically. (B) Pixel map of the NeuroCCD-SM camera depicting, in red, the area of interest. (C) Experimental protocol. (D) Spatially averaged optical outputs from the red pixels in B (represented by bars whose heights indicate the amplitude of the voltage change under each experimental condition in the row labelled 'Ganglion') and from the pixels that outline individual neurones ('Cells'). Magnification, 100×. 'Ganglion' signals were high-pass filtered at 6.6 Hz. 'Cell' traces were unfiltered.

Discussion

Studies of nAChRs in the ENS provide a natural link between events at the molecular and cellular level and the

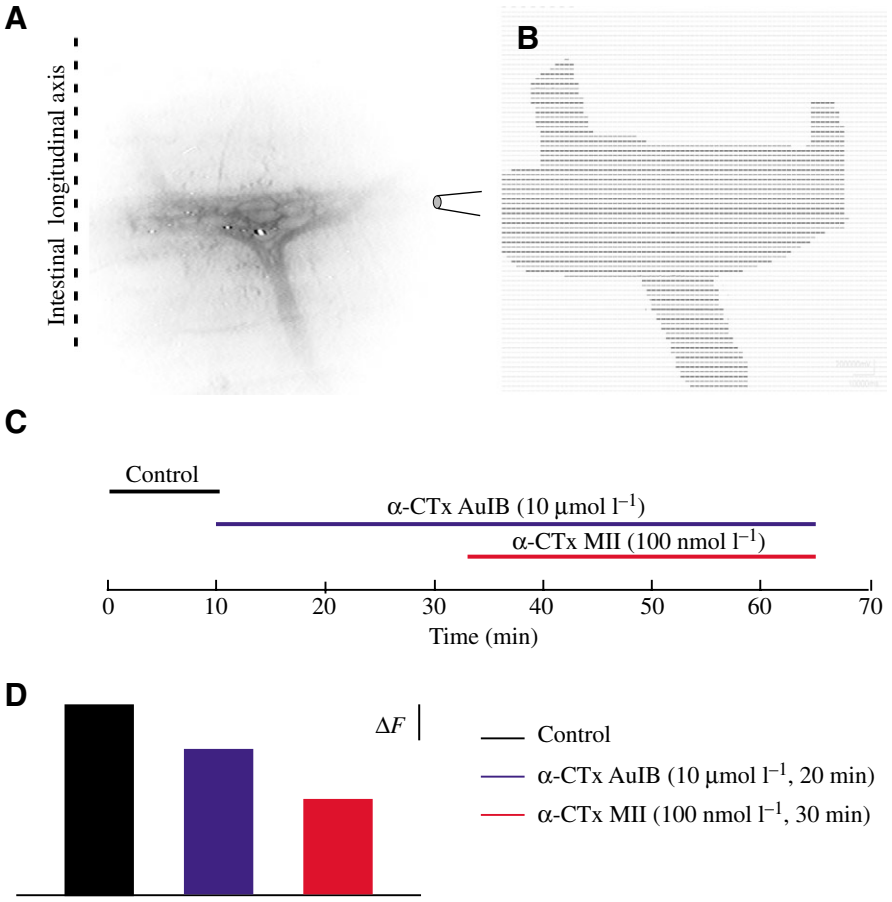

Fig. 9. The effects of α-CTx AuIB and α-CTx MII on submucosal ganglia can be reproduced on myenteric ganglia, confirming that α3β2- and α3β4-containing nAChRs are expressed in both enteric plexuses. (A) High-resolution image of a myenteric ganglion (inverted grey scale). The position of the stimulation electrode is shown schematically. (B) Pixel map of the NeuroCCD-SM camera depicting, in dark grey, the area of interest. Notice that the highlighted area is considerably bigger than the ganglion itself. (C) Experimental protocol. (D) Spatially averaged optical outputs from the dark-grey pixels in B, represented by bars whose heights indicate the amplitude of the voltage change under each experimental condition. Magnification, 40×. All signals were high-pass filtered at 9.8 Hz.

dynamics of synaptic interactions within the network; the results presented here illustrate this connection. In general, we have found that a range of nAChR-subunits, with the exception of α4, is present in enteric ganglia, as determined by RIAs, immunocytochemistry and selective nicotinic blockers. However, the proportional expression of these subunits is different in the submucous and myenteric plexuses, and the lack of α4 is in stark contrast with its abundance in brain.

A detailed analysis of the radioimmunoassay data summarized in Table 2 indicates the following.

(1) In detergent extracts from guinea-pig brain as well as from guinea-pig intestine, our mAbs revealed the presence of nAChRs that contain α7-subunits and bind αBgT, as well as nAChRs that contain α3-, α4-, α5-, β2- and β4-subunits and bind epibatidine.

(2) The relative binding of mAb 299 shows that α4-nAChRs are much more abundant in guinea-pig brain than in guinea-pig gut.

(3) The relative binding of mAb 313 shows that α3-nAChRs are much more abundant in guinea-pig gut than in guinea-pig brain. However, mAb 313 does not recognize guinea-pig α3 as well as mAb 210 does.

(4) Since α5 is always found in combination with other α-subunits (e.g. α3, α4 or α6), the amount of nAChR bound by mAb 210 is the total of α3- plus other α5-containing nAChRs. In brain, α4β2α5-nAChRs represent up to 25% of the total α4β2-nAChRs (Gerzanich et al., 1998); but in enteric ganglia, where α4-nAChRs are practically absent, mAb 210 must be predominantly bound to α3-nAChRs.

(5) In the same extracts, mAb 306 immunoreacts with a protein that binds αBgT, a selective ligand for α7-nAChRs. Since saturation-binding curves of αBgT to nAChRs immuno-isolated on mAb306 from guinea-pig brain mimic the typical binding curve for homomeric α7-nAChRs (results not shown; Anand et al., 1993), it follows that mAb 306 must react specifically with guinea-pig α7-nAChRs. Indeed, as demonstrated previously in mammalian brain (Lindstrom, 2000a), α7-nAChRs and α4β2-nAChRs appear to be the predominant nAChR-subtypes in guinea-pig brain.

(6) The binding of mAb 295 indicates that β2-subunits are present in both guinea-pig brain and gut. Approximately half (66 pmol kg^{-1} *vs* 140 pmol kg^{-1}; Table 2) of the α3-containing nAChRs in the small intestine contain β2-subunits.

(7) The binding of mAb 337 indicates that β4-nAChRs are also present in both tissues. However, the data show that only 0.7% (1.0 pmol kg^{-1} *vs* 140 pmol kg^{-1}; Table 2) of intestinal α3-nAChRs were precipitated by an mAb to human β4-subunits. Since the sum of β2-containing (66 pmol kg^{-1}) and β4-containing (1.0 pmol kg^{-1}) nAChRs in the intestine does not equal the total amount of α3-nAChRs (140 pmol kg^{-1}), poor guinea-pig epitope recognition by one or both of these mAbs must limit the extent of binding. Indeed, β4-subunits

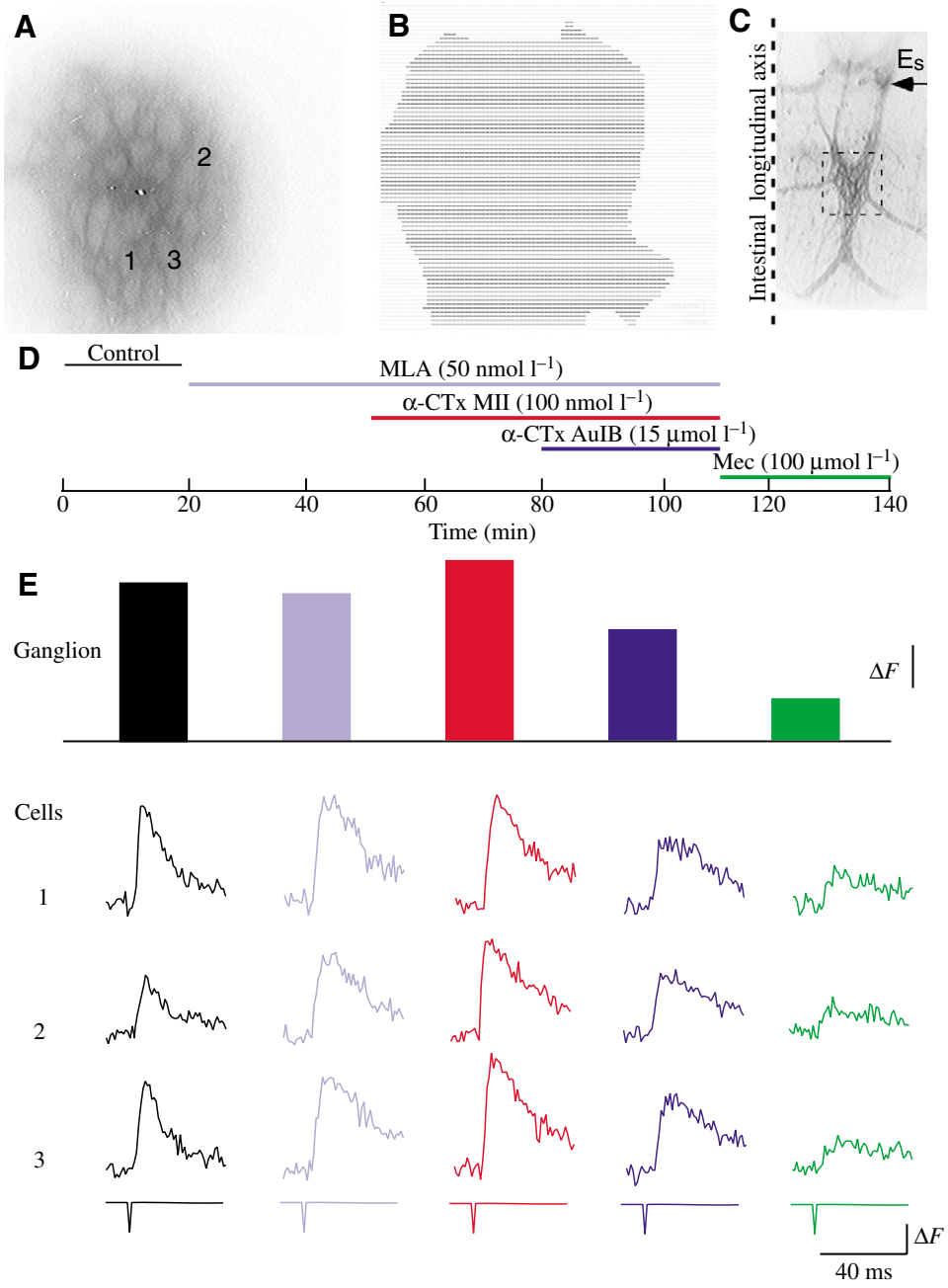

Fig. 10. nAChR antagonists can also enhance synaptically evoked responses in the myenteric plexus. (A) High-resolution image of a myenteric ganglion (inverted grey scale), showing three individual neurones identified by numbers. (B) Pixel map of the NeuroCCD-SM camera depicting, in dark grey, the area of interest. Notice that, as in Fig. 8, the highlighted area is considerably bigger than the ganglion itself. (C) Low-magnification image of the preparation (20×), illustrating the location of the stimulating electrode (E_s) with respect to the recording area. (D) Experimental protocol. (E) Spatially averaged optical outputs from the dark-grey pixels in B (represented by bars whose heights indicate the amplitude of the voltage change under each experimental condition in the row labelled 'Ganglion') and from the pixels that outline neurones 1, 2 and 3 ('Cells'). Magnification, 100×. 'Ganglion' signals were high-pass filtered at 6.6 Hz. 'Cell' traces were unfiltered.

must be underestimated as a consequence of the limited recognition by mAb 337 (Nelson et al., 2001) and because half of the α3-nAChRs that were not bound by mAb 295 to β2 must contain the β4-subunit. mAb 295 can bind at least 47% of intestinal α3-nAChRs, indicating clearly that the ENS contains a substantial amount of α3β2-nAChRs. Indeed, pharmacological experiments that we performed on submucous- and myenteric-plexus preparations (see below) demonstrated the functional contribution of α3β2- and α3β4-containing nAChRs to synaptic signalling in these neuronal networks.

From these results, two important conclusions follow: (1) all subunits tested are present in both brain and gut, with the exception of α4, which, although abundant in brain, is virtually absent in the gut and (2) ligands such as αBgt and epibatidine, of unquestioned specificity for neuronal nAChR-subtypes in other species, recognize the same targets in the guinea-pig neurones. These findings demonstrate unequivocally that the nAChRs of the guinea pig are not significantly different from those in other well-studied biological systems in their affinity for specific ligands and in their recognition by mAbs and they validate these mAbs as powerful tools for immunocytochemical studies of nAChRs in the guinea-pig ENS.

To determine which nAChR-subunits co-localize, and to reveal the spatial distribution of the various nAChR subtypes,

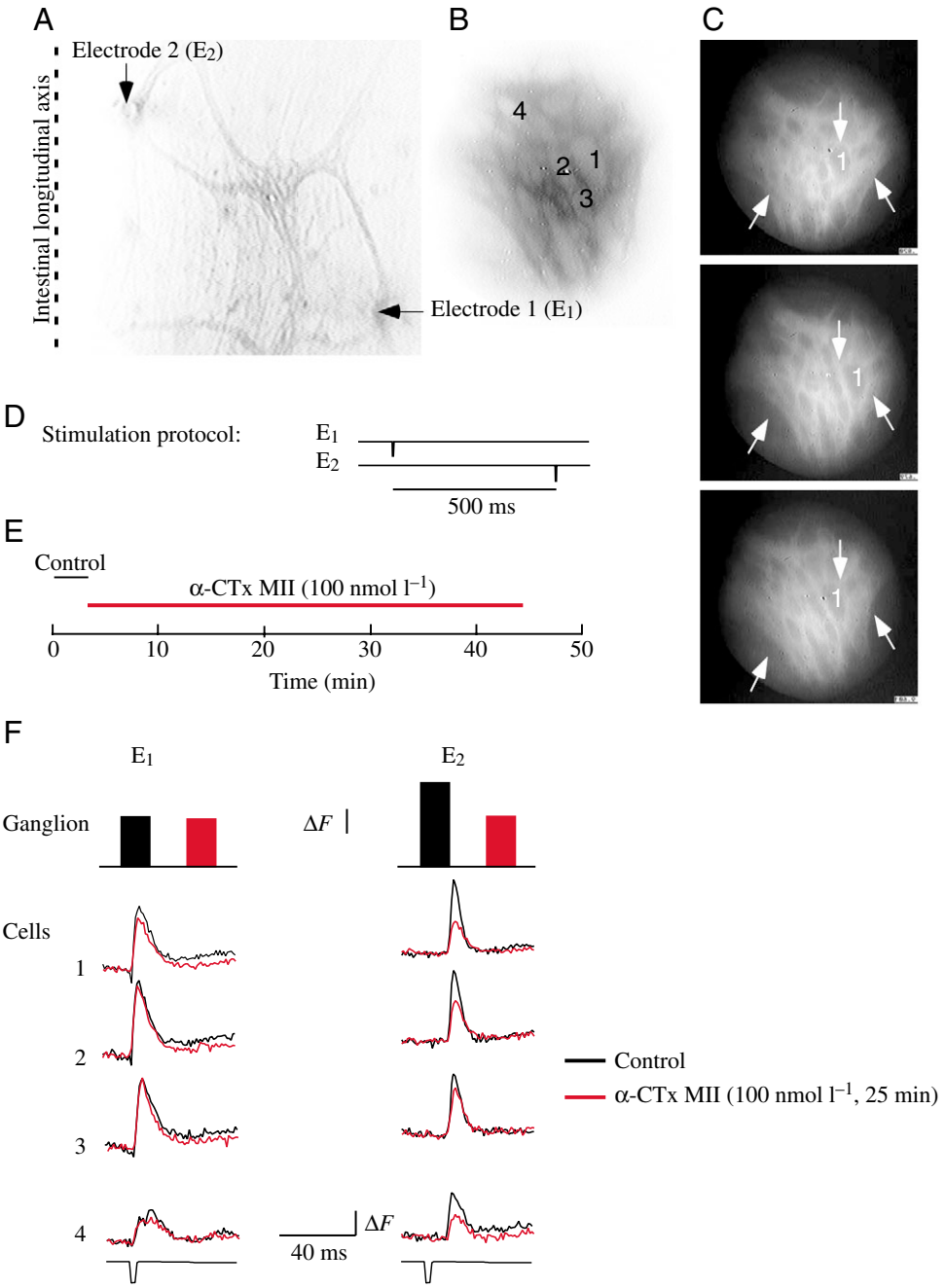

Fig. 11. Myenteric neurones exhibit differential pharmacological responses to a given nAChR antagonist depending upon the location of the stimulation electrode, oral or aboral with respect to the ganglion. (A) Low-magnification image of the preparation (20×), illustrating the location of the stimulating electrodes (E_1 and E_2) with respect to the recording area. (B) High-resolution image of the myenteric ganglion of interest (inverted grey scale), showing four individual neurones identified by numbers. (C) Serial images of the selected myenteric ganglion taken at 20 min intervals throughout the experiment. Notice the changes in ganglion shape (and therefore in registration with respect to the camera) from one frame to another. The arrows have been inserted as fixed references to draw attention to the magnitude of the ganglionic movements. Magnification, 100×. (D) Stimulation protocol. (E) Experimental protocol. (F) Optical responses evoked by each of the stimulation electrodes (E_1 and E_2) according to the protocol described in D. Data are presented in two ways: signals spatially averaged over the whole ganglion (row of bars labelled 'Ganglion', whose heights represent the amplitude of the voltage change evoked by each electrode, averaged over the area of interest) and signals spatially averaged over individual neurones ('Cells' numbered 1–4). (G) High-speed camera movies showing the spatial pattern of responses to stimulation by electrodes E_1 and E_2, before and after 25 min exposure to 100 nmol l^{-1} α-CTx MII. Frame acquisition 1 kHz. Unfiltered.

we applied immunofluorescence techniques and the mAbs to nAChR-subunits listed in Table 1 to whole mounts of submucous and myenteric plexuses. The results of Fig. 1 strongly suggest that α3-subunits are the predominant α-

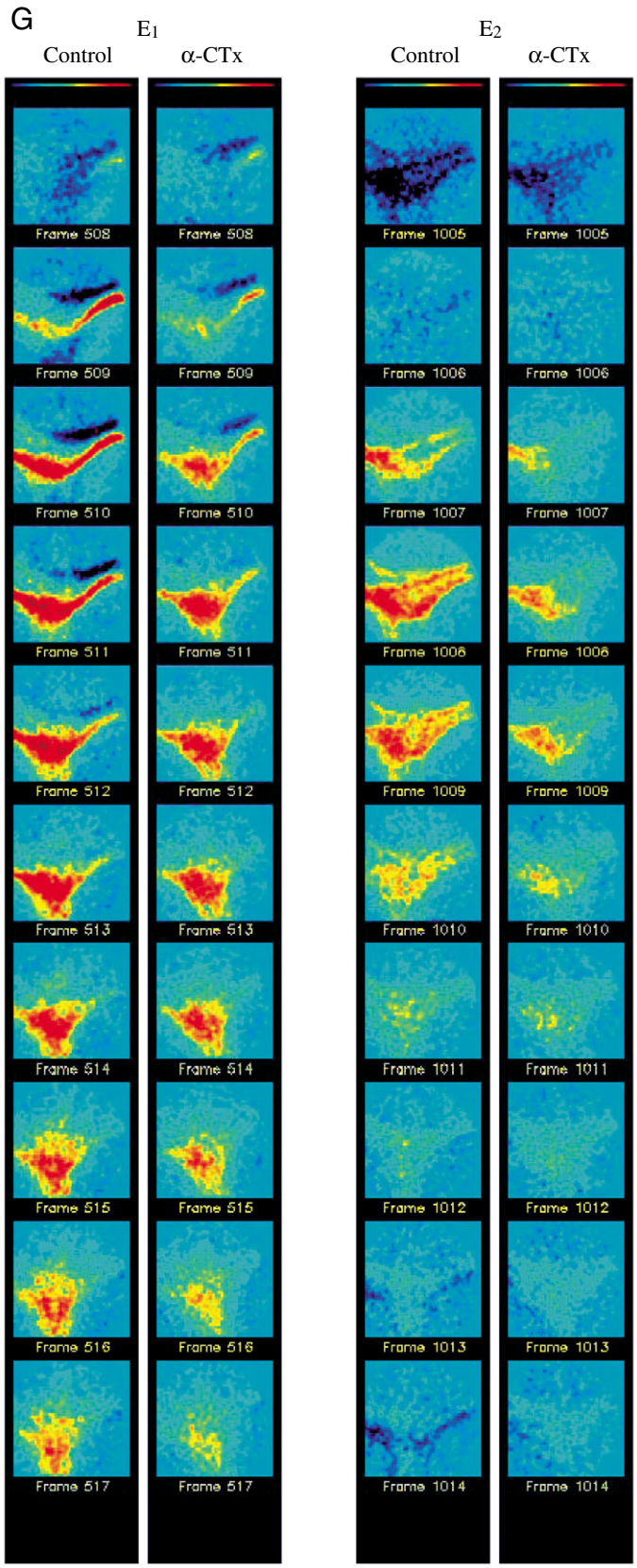

Fig. 11G. See previous page for legend.

subunits in heteromeric nAChRs, and Figs 2 and 3 establish the expression of α7-nAChRs in all enteric ganglia. Note, however, that α7 expression in myenteric ganglia is relatively sparse. The relative scarcity of myenteric neurones expressing α7-nAChRs may explain electrophysiological studies (Zhou et al., 2002) that concluded that α7-antagonists, such as αBgT (0.1 μmol l^{-1}) and MLA (0.1 μmol l^{-1}), did not affect ACh-induced responses in isolated myenteric neurones in culture[†]. The predominance of α3β2-nAChRs that we found using immunocytochemical methods (Fig. 4), on the other hand, is similar to that obtained by Bibevski et al. (2000) in canine intra-cardiac ganglia. Indeed, employing several of the same mAbs used in this report (e.g. mAb 210, mAb 313 and mAb 295) in conjunction with electrophysiological and pharmacological assays specific for α3β2 or α3β4, respectively, these authors determined that functional ganglionic transmission in canine intra-cardiac ganglia is primarily mediated by α3β2-nAChRs (Bibevski et al., 2000).

Heteromeric nAChRs formed from combinations of α3-, β2-, β4- and α5-subunits are found in chicken ciliary ganglion neurones (Conroy and Berg, 1995) and in some human neuroblastoma cell lines (Nelson et al., 2001; Peng et al., 1997). Further, functional experiments carried out both in isolated myenteric neurones (Galligan, 1999; Galligan and North, 2004; Wang et al., 2003; Zhou et al., 2002) and in intact enteric plexus preparations (see Results) strongly suggest a role for β4-containing nAChRs in gastrointestinal physiology. Therefore, we expected to find immunocytochemical evidence for β4 expression in enteric ganglia. Although this prediction was weakly confirmed by liquid-phase RIAs using mAb 337 with small-intestine extracts (see Table 2), the labelling of the whole mounts of submucous and myenteric plexuses with mAb 337 (not shown) yielded only a very faint, diffuse pattern of immunoreactivity. Once again, the discrepancy between the profound pharmacological effects of β4-agonists and antagonists observed during functional experiments, and the apparently weak expression of β4-nAChRs indicated by mAb 337 binding, might be explained by limited recognition of this mAb for the guinea-pig β4-nAChRs, or by lack of accessibility to the epitope due to steric factors.

To demonstrate the role of the different nAChR-subtypes in the functional connectivity of the enteric networks, we combined MSORTV and pharmacology. The main results

[†]There is strong evidence that native α7-nAChRs are homo-pentamers (see, for example, Chen and Patrick, 1997; Drisdel and Green, 2000). However, in expression systems, α7-subunits have been shown to combine with β2-subunits (Khiroug et al., 2002) to form functional nAChRs, raising the possibility that they could also exist as hetero-pentamers (Azam et al., 2003). Although we have immunocytochemical data confirming expression of α7- and β2-subunits in the same enteric neurons (not shown), we have no independent evidence of co-localization in the same nAChR molecule. Furthermore, the presence of α7-isoforms 1 and 2 (Severance et al., 2004) in the ENS remains an open question. Since they differ in their extracellular domain, we could not have distinguished them with mAb 306, which recognizes an intracellular epitope; and since we did not use α-Bgt for functional studies, we could not assess their individual contributions to the overall α7-nAChR pool on the basis of their differential affinities for this toxin. We also considered the possibility of additional α-subunits being expressed in enteric neurons. However, α8-nAChRs have only been found in avians, and the lack of specific probes for α9- and α10-nAChRs precluded investigation of their expression in the guinea-pig ENS.

obtained on the submucous plexus are shown in Figs 5–8. Those experiments that employed specific antagonists of nAChR-subtypes (α-CTx MII for α3β2, α-CTx AuIB for α3β4 and MLA for α7) and Mec, a non-competitive antagonist of all nAChRs, revealed that nAChR expression varies from neurone to neurone but that, on average, all the expected nAChRs subtypes are present in every ganglion and contribute to the synaptic responses to stimulation. This is illustrated in Fig. 6C, where selected cells of the ganglion under study exhibit several distinct pharmacological profiles (see below).

Cell 2. Its evoked synaptic response was reduced by α-CTx MII, revealing the presence of α3β2- and/or α3β2β4-nAChRs. Further reduction by α-CTx AuIB indicates that this neurone also expressed α3β4-nAChRs as independent entities. The fact that Mec completely eliminated the response remaining after the block of all α3-containing nAChRs implies that most, if not all, the incoming inputs into this cell activated nAChRs and that the residual response blocked by Mec was mediated, primarily, by α7-nAChRs.

Cell 4. Its pharmacological profile suggests that this neurone expressed α7- and/or other nAChRs not yet identified and, in addition, it expressed receptors to other excitatory, non-cholinergic neurotransmitters.

Cell 10. This result underscores the lack of activation of α3β4-nAChRs. The further, but still incomplete, block of the response by Mec implies the expression of α7- and/or other nAChRs, as well as non-nicotinic receptors.

The role of non-nicotinic receptors (in particular, purinergic and serotonergic) in the generation of excitatory postsynaptic potentials has been extensively investigated in submucous (see, for example, Barajas-Lopez et al., 2000; Hu et al., 2003; Monro et al., 2004; Surprenant and Crist, 1988) as well as in myenteric (see, for example, Barajas-Lopez et al., 1993; LePard and Galligan, 1999; LePard et al., 1997; Nurgali et al., 2003; Zhou and Galligan, 1999) plexuses. Our experiments were intended to fill the information void that surrounds enteric nAChRs with regard to the expression and function of their different subtypes.

In the majority of the submucosal ganglia examined, the α-CTx's effects were additive, suggesting that most of the α3β2- and α3β4-nAChRs exist as independent entities rather than as part of $(\alpha3)_2(\beta2)_x(\beta4)_y$-nAChRs. The differential sensitivity of individual cells to these toxins indicates varied levels of expression of β2- and β4-nAChR subtypes within different neurones, in agreement with our immunocytochemistry (see, for example, Fig. 4 for a ganglion expressing β2-containing nAChRs), and may also reflect the strength of the particular synaptic inputs activated by a given stimulus. In addition, the significant reduction in the magnitude of the evoked response caused by α-CTx AuIB in several neurones (e.g. five of 15 in the ganglion depicted in Fig. 7) confirmed that β4-containing nAChRs play a substantial role in fast synaptic transmission within the submucous plexus.

Fig. 8 illustrates an experiment in which α7-nAChRs were blocked with MLA prior to the addition of α-CTx MII. Under these circumstances, the reduction in the magnitude of the synaptic response due to the α-CTx MII treatment was smaller than that observed in the absence of MLA. This result is consistent with a role for α7-nAChRs as both mediators of transmission and modulators of transmitter release in the enteric nervous system.

Optical signals obtained with voltage-sensitive dyes, and optically recorded synaptic responses in particular, are difficult to quantitate (Salzberg, 1983). Our experiments clearly show that the magnitude of the evoked fast epsps depends upon receptor expression, synaptic strength and stimulus intensity. However, parameters not easily quantifiable under our experimental conditions – e.g. amount of dye bound to the neuronal membrane, membrane area and resting potential of individual neurones – also critically affect the size of the optical signal, preventing a quantitative cell-to-cell comparison of pharmacological profiles. Normalization of control signals may reduce some of these uncertainties, but this procedure still exempts nAChRs that, although expressed in the cell membrane, may be unaffected by a particular incoming stimulus that enters the ganglion through one, or at most two, of the multiple ganglionic connectives. For these reasons, we have here avoided quantitating the relative distribution of nAChR-subtypes identified in our studies. The alternative way of exhibiting the results, spatial-averages of the optical signals over entire ganglia, manifests the same limitations characteristic of single-cell analysis but it provides a quick, qualitative survey of the results of a given experiment. In addition, it is extremely useful when studying myenteric ganglia, in which the majority of the neurones cannot be monitored individually.

In the myenteric plexus, blocking nAChRs over an intact segment yields differential responses in a given ganglion, depending upon the location of the stimulus, oral or aboral from the ganglion of interest, along the longitudinal axis of the gut. This finding suggests that the functional outputs of individual neurones in intact preparations, as well as their responses to the nAChR blockers, are moulded by the inputs they receive and that the anisotropy of the myenteric plexus architecture relative to that of the submucous plexus accentuates this effect. In particular, while the neuronal projections in the submucous plexus are relatively short ($\leqslant$3 mm) and symmetrical along the longitudinal axis (Song et al., 1992), the projections for sensory neurones and interneurones in the myenteric plexus are short in the oral direction ($\leqslant$10–20 mm) but very long in the aboral direction ($\geqslant$110–120 mm) (Brookes et al., 1997; Song et al., 1996, 1997b, 1998). Furthermore, the different classes of interneurones in ascending and descending pathways may contribute to the intrinsic directionality of the myenteric plexus (Costa et al., 1996). This directionality, together with differential nAChR-subtype expression, may, in turn, influence the pharmacological characteristics of the responses. Indeed, our observation of a variety of activity patterns that follows sequential elimination of individual nAChR-subtypes in the myenteric plexus (Figs 9–11) suggests that nAChRs may be capable of regulating the activity of both excitatory and

inhibitory pathways. This interpretation, although only tentative because of the non-specific electrical stimulation of fibre tracts, is truly tantalizing, as a similar role has been widely recognized for nAChRs in the central nervous system (Alkondon et al., 1999, 2000; Cordero-Erausquin et al., 2004; Ji and Dani, 2000; Takeda et al., 2003). In fact, if proven true, it may uncover a new functional role for the enteric nAChRs in the larger context of the integrative circuitry.

In summary, we have here combined RIAs and confocal microscopy with the use of mAbs to identify and localize the different nAChR-subunits present in enteric neurones. At the molecular level, we were able to show that α3β2-, α3β4-, α3β2β4- and α7-nAChR subtypes are expressed in both submucosal and myenteric plexuses. At the cellular level, we determined that nAChR expression varies from neurone to neurone but that, on average, all are present in every ganglion and could contribute to the synaptic responses to stimulation. At the network level, we took advantage of the quasi-two-dimensional architecture of the guinea-pig ENS and we combined MSORTV and specific nAChR-antagonists to demonstrate that several subtypes play functional roles in both enteric plexuses.

This work was supported by United States Public Health Service grants NS16824 (B.M.S.) and NS11323 (J.L.) and the Philip Morris External Research Program (J.L.). We are extremely grateful to Dr J. Michael McIntosh for his generous gift of α-CTx MII and α-CTx AuIB, to Drs Alan Gelperin, Paul DeWeer and Simon Brookes for their thoughtful comments on an earlier version of the manuscript and to John Cooper for valuable technical assistance.

References

Alkondon, M., Pereira, E. F., Wonnacott, S. and Albuquerque, E. X. (1992). Blockade of nicotinic currents in hippocampal neurons defines methyllycaconitine as a potent and specific receptor antagonist. *Mol. Pharmacol.* **41**, 802-808.

Alkondon, M., Pereira, E. F., Eisenberg, H. M. and Albuquerque, E. X. (1999). Choline and selective antagonists identify two subtypes of nicotinic acetylcholine receptors that modulate GABA release from CA1 interneurons in rat hippocampal slices. *J. Neurosci.* **19**, 2693-2705.

Alkondon, M., Pereira, E. F., Eisenberg, H. M. and Albuquerque, E. X. (2000). Nicotinic receptor activation in human cerebral cortical interneurons: a mechanism for inhibition and disinhibition of neuronal networks. *J. Neurosci.* **20**, 66-75.

Anand, R., Peng, X. and Lindstrom, J. (1993). Homomeric and native alpha 7 acetylcholine receptors exhibit remarkably similar but non-identical pharmacological properties, suggesting that the native receptor is a heteromeric protein complex. *FEBS Lett.* **327**, 241-246.

Azam, L., Winzer-Serhan, U. and Leslie, F. M. (2003). Co-expression of alpha7 and beta2 nicotinic acetylcholine receptor subunit mRNAs within rat brain cholinergic neurons. *Neuroscience* **119**, 965-977.

Barajas-Lopez, C., Barrientos, M. and Espinosa-Luna, R. (1993). Suramin increases the efficacy of ATP to activate an inward current in myenteric neurons from guinea-pig ileum. *Eur. J. Pharmacol.* **250**, 141-145.

Barajas-Lopez, C., Espinosa-Luna, R. and Christofi, F. L. (2000). Changes in intracellular Ca2+ by activation of P2 receptors in submucosal neurons in short-term cultures. *Eur. J. Pharmacol.* **409**, 243-257.

Bayliss, W. M. and Starling, E. H. (1899). The movements and innervation of the small intestine. *J. Physiol.* **24**, 99-143.

Bibevski, S., Zhou, Y., McIntosh, J. M., Zigmond, R. E. and Dunlap, M. E. (2000). Functional nicotinic acetylcholine receptors that mediate ganglionic transmission in cardiac parasympathetic neurons. *J. Neurosci.* **20**, 5076-5082.

Bornstein, J. C. and Furness, J. B. (1988). Correlated electrophysiological and histochemical studies of submucous neurons and their contribution to understanding enteric neural circuits. *J. Auton. Nerv. Syst.* **25**, 1-13.

Bornstein, J. C., Furness, J. B., Smith, T. K. and Trussell, D. C. (1991). Synaptic responses evoked by mechanical stimulation of the mucosa in morphologically characterized myenteric neurons of the guinea-pig ileum. *J. Neurosci.* **11**, 505-518.

Brookes, S. J., Meedeniya, A. C., Jobling, P. and Costa, M. (1997). Orally projecting interneurones in the guinea-pig small intestine. *J. Physiol.* **505**, 473-491.

Cartier, G. E., Yoshikami, D., Gray, W. R., Luo, S., Olivera, B. M. and McIntosh, J. M. (1996). A new alpha-conotoxin which targets alpha3beta2 nicotinic acetylcholine receptors. *J. Biol. Chem.* **271**, 7522-7528.

Chen, D. and Patrick, J. W. (1997). The alpha-bungarotoxin-binding nicotinic acetylcholine receptor from rat brain contains only the alpha7 subunit. *J. Biol. Chem.* **272**, 24024-24029.

Colquhoun, L. M. and Patrick, J. W. (1997). Pharmacology of neuronal nicotinic acetylcholine receptor subtypes. *Adv. Pharmacol.* **39**, 191-220.

Conroy, W. G. and Berg, D. K. (1995). Neurons can maintain multiple classes of nicotinic acetylcholine receptors distinguished by different subunit compositions. *J. Biol. Chem.* **270**, 4424-4431.

Cordero-Erausquin, M., Pons, S., Faure, P. and Changeux, J. P. (2004). Nicotine differentially activates inhibitory and excitatory neurons in the dorsal spinal cord. *Pain* **109**, 308-318.

Costa, M., Brookes, S. J., Steele, P. A., Gibbins, I., Burcher, E. and Kandiah, C. J. (1996). Neurochemical classification of myenteric neurons in the guinea-pig ileum. *Neuroscience* **75**, 949-967.

Dominguez del Toro, E., Juiz, J. M., Peng, X., Lindstrom, J. and Criado, M. (1994). Immunocytochemical localization of the alpha 7 subunit of the nicotinic acetylcholine receptor in the rat central nervous system. *J. Comp. Neurol.* **349**, 325-342.

Drisdel, R. C. and Green, W. N. (2000). Neuronal alpha-bungarotoxin receptors are alpha7 subunit homomers. *J. Neurosci.* **20**, 133-139.

Fabian-Fine, R., Skehel, P., Errington, M. L., Davies, H. A., Sher, E., Stewart, M. G. and Fine, A. (2001). Ultrastructural distribution of the alpha7 nicotinic acetylcholine receptor subunit in rat hippocampus. *J. Neurosci.* **21**, 7993-8003.

Furness, J. B. and Costa, M. (1987). *The Enteric Nervous System*. New York: Churchill Livingstone.

Galligan, J. J. (1999). Nerve terminal nicotinic cholinergic receptors on excitatory motoneurons in the myenteric plexus of guinea pig intestine. *J. Pharmacol. Exp. Ther.* **291**, 92-98.

Galligan, J. J. and North, R. A. (2004). Pharmacology and function of nicotinic acetylcholine and P2X receptors in the enteric nervous system. *Neurogastroenterol. Motil.* **1**, 64-70.

Gerzanich, V., Wang, F., Kuryatov, A. and Lindstrom, J. (1998). alpha 5 Subunit alters desensitization, pharmacology, Ca^{++} permeability and Ca^{++} modulation of human neuronal alpha 3 nicotinic receptors. *J. Pharmacol. Exp. Ther.* **286**, 311-320.

Green, J. T., Thomas, G. A., Rhodes, J., Evans, B. K., Russell, M. A., Feyerabend, C., Fuller, G. S., Newcombe, R. G. and Sandborn, W. J. (1997a). Pharmacokinetics of nicotine carbomer enemas: a new treatment modality for ulcerative colitis. *Clin. Pharmacol. Ther.* **61**, 340-348.

Green, J. T., Thomas, G. A., Rhodes, J., Williams, G. T., Evans, B. K., Russell, M. A., Feyerabend, C., Rhodes, P. and Sandborn, W. J. (1997b). Nicotine enemas for active ulcerative colitis–a pilot study. *Aliment. Pharm. Therap.* **11**, 859-863.

Hirst, G. D. and McKirdy, H. C. (1975). Synaptic potentials recorded from neurones of the submucous plexus of guinea-pig small intestine. *J. Physiol.* **249**, 369-385.

Hu, H. Z., Gao, N., Zhu, M. X., Liu, S., Ren, J., Gao, C., Xia, Y. and Wood, J. D. (2003). Slow excitatory synaptic transmission mediated by P2Y1 receptors in the guinea-pig enteric nervous system. *J. Physiol.* **550**, 493-504.

Hubel, K. A., Renquist, K. S. and Varley, G. (1991). Secretory reflexes in ileum and jejunum: absence of remote effects. *J. Auton. Nerv. Syst.* **35**, 53-62.

Ji, D. and Dani, J. A. (2000). Inhibition and disinhibition of pyramidal neurons by activation of nicotinic receptors on hippocampal interneurons. *J. Neurophysiol.* **83**, 2682-2690.

Khiroug, S. S., Harkness, P. C., Lamb, P. W., Sudweeks, S. N., Khiroug, L., Millar, N. S. and Yakel, J. L. (2002). Rat nicotinic ACh receptor alpha7

and beta2 subunits co-assemble to form functional heteromeric nicotinic receptor channels. *J. Physiol.* **540**, 425-434.

Kirchgessner, A. L. and Liu, M. T. (1998). Immunohistochemical localization of nicotinic acetylcholine receptors in the guinea pig bowel and pancreas. *J. Comp. Neurol.* **390**, 497-514.

LePard, K. J. and Galligan, J. J. (1999). Analysis of fast synaptic pathways in myenteric plexus of guinea pig ileum. *Am J. Physiol.* **276**, G529-G538.

LePard, K. J., Messori, E. and Galligan, J. J. (1997). Purinergic fast excitatory postsynaptic potentials in myenteric neurons of guinea pig: distribution and pharmacology. *Gastroenterology* **113**, 1522-1534.

Lindstrom, J. (2000a). The structure of neuronal nicotinic receptors. In *Neuronal Nicotinic Receptors* (ed. F. Clementi, C. Gotti and D. Fornasari), pp. 101-162. New York: Springer.

Lindstrom, J. M. (2000b). Acetylcholine receptors and myasthenia. *Muscle Nerve* **23**, 453-477.

Lindstrom, J. M., Seybold, M. E., Lennon, V. A., Whittingham, S. and Duane, D. D. (1976). Antibody to acetylcholine receptor in myasthenia gravis. Prevalence, clinical correlates, and diagnostic value. *Neurology* **26**, 1054-1059.

Lindstrom, J., Anand, R., Gerzanich, V., Peng, X., Wang, F. and Wells, G. (1996). Structure and function of neuronal nicotinic acetylcholine receptors. *Prog. Brain Res.* **109**, 125-137.

Luo, S., Kulak, J. M., Cartier, G. E., Jacobsen, R. B., Yoshikami, D., Olivera, B. M. and McIntosh, J. M. (1998). alpha-conotoxin AuIB selectively blocks alpha3 beta4 nicotinic acetylcholine receptors and nicotine-evoked norepinephrine release. *J. Neurosci.* **18**, 8571-8579.

McLane, K. E., Wu, X., Lindstrom, J. M. and Conti-Tronconi, B. M. (1992). Epitope mapping of polyclonal and monoclonal antibodies against two alpha-bungarotoxin-binding alpha subunits from neuronal nicotinic receptors. *J. Neuroimmunol.* **38**, 115-128.

Monro, R. L., Bertrand, P. P. and Bornstein, J. C. (2004). ATP participates in three excitatory postsynaptic potentials in the submucous plexus of the guinea pig ileum. *J. Physiol.* **556**, 571-584.

Moore, B. A. and Vanner, S. (1998). Organization of intrinsic cholinergic neurons projecting within submucosal plexus of guinea pig ileum. *Am J. Physiol.* **275**, G490-G497.

Moore, B. A. and Vanner, S. (2000). Properties of synaptic inputs from myenteric neurons innervating submucosal S neurons in guinea pig ileum. *Am J. Physiol. Gastrointest. Liver Physiol.* **278**, G273-G280.

Nelson, M. E., Wang, F., Kuryatov, A., Choi, C. H., Gerzanich, V. and Lindstrom, J. (2001). Functional properties of human nicotinic AChRs expressed by IMR-32 neuroblastoma cells resemble those of alpha3beta4 AChRs expressed in permanently transfected HEK cells. *J. Gen. Physiol.* **118**, 563-582.

Neunlist, M., Peters, S. and Schemann, M. (1999). Multisite optical recording of excitability in the enteric nervous system. *Neurogastroenterol. Motil.* **11**, 393-402.

Nurgali, K., Furness, J. B. and Stebbing, M. J. (2003). Analysis of purinergic and cholinergic fast synaptic transmission to identified myenteric neurons. *Neuroscience* **116**, 335-347.

Obaid, A. L. and Lindstrom, J. (2000). AChR subunits expressed in enteric ganglia: immunohystochemical identification and localization. *Auton. Neurosc.* **82**, 70.

Obaid, A. L., Zou, D.-J., Rohr, S. and Salzberg, B. M. (1992). Optical recording with single cell resolution from a simple mammalian nervous system: Electrical activity in ganglia from the submucous plexus of the guinea-pig ileum. *Biol. Bull.* **183**, 344-346.

Obaid, A. L., Koyano, T., Lindstrom, J., Sakai, T. and Salzberg, B. M. (1999a). Spatiotemporal patterns of activity in an intact mammalian network with single-cell resolution: optical studies of nicotinic activity in an enteric plexus. *J. Neurosci.* **19**, 3073-3093.

Obaid, A. L., Wells, G. B., Kuryatov, A. and Lindstrom, J. (1999b). nAChR subunits that mediate nicotinic activity in the enteric nervous system. *Soc. Neurosci. Abstr.* **25**, 1490a.

Obaid, A. L., Cooper, J. F. and Lindstrom, J. (2001). Nicotinic Receptors in guinea pig gut: Validation of monoclonal antibody specificity. *Neurosci. Abstr.* **31**, A374.11.

Obaid, A. L., Loew, L. M., Wuskell, J. P. and Salzberg, B. M. (2004). Novel naphthylstyryl-pyridinium potentiometric dyes offer advantages for neural network analysis. *J. Neurosci. Methods* **134**, 179-190.

Osborne, M. J. and Stansby, G. (1994). Smoking and chronic inflammatory bowel disease. *J. Roy. Soc. Health* **114**, 317-319.

Parsons, T. D., Salzberg, B. M., Obaid, A. L., Raccuia-Behling, F. and Kleinfeld, D. (1991). Long-term optical recording of patterns of electrical activity in ensembles of cultured Aplysia neurons. *J. Neurophysiol.* **66**, 316-333.

Peng, X., Gerzanich, V., Anand, R., Wang, F. and Lindstrom, J. (1997). Chronic nicotine treatment up-regulates alpha3 and alpha7 acetylcholine receptor subtypes expressed by the human neuroblastoma cell line SH-SY5Y. *Mol. Pharmacol* **51**, 776-784.

Reed, D. E. and Vanner, S. J. (2003). Long vasodilator reflexes projecting through the myenteric plexus in guinea-pig ileum. *J. Physiol.* **553**, 911-924.

Salzberg, B. M. (1983). Optical recording of electrical activity in neurons using molecular probes. In *Current Methods in Cellular Neurobiology* (ed. J. Barker and J. McKelvy), pp. 139-187. New York: John Wiley & Sons.

Salzberg, B. M., Grinvald, A., Cohen, L. B., Davila, H. V. and Ross, W. N. (1977). Optical recording of neuronal activity in an invertebrate central nervous system: simultaneous monitoring of several neurons. *J. Neurophysiol.* **40**, 1281-1291.

Schemann, M., Michel, K., Peters, S., Bischoff, S. C. and Neunlist, M. (2002). Cutting-edge technology. III. Imaging and the gastrointestinal tract: mapping the human enteric nervous system. *Am J. Physiol. Gastrointest. Liver Physiol.* **282**, G919-G925.

Schoepfer, R., Conroy, W. G., Whiting, P., Gore, M. and Lindstrom, J. (1990). Brain alpha-bungarotoxin binding protein cDNAs and MAbs reveal subtypes of this branch of the ligand-gated ion channel gene superfamily. *Neuron* **5**, 35-48.

Severance, E. G., Zhang, H., Cruz, Y., Pakhlevaniants, S., Hadley, S. H., Amin, J., Wecker, L., Reed, C. and Cuevas, J. (2004). The alpha7 nicotinic acetylcholine receptor subunit exists in two isoforms that contribute to functional ligand-gated ion channels. *Mol. Pharmacol.* **66**, 420-429.

Song, Z. M., Brookes, S. J., Steele, P. A. and Costa, M. (1992). Projections and pathways of submucous neurons to the mucosa of the guinea-pig small intestine. *Cell Tissue Res.* **269**, 87-98.

Song, Z., Brookes, S. J. and Costa, M. (1996). Projections of specific morphological types of neurons within the myenteric plexus of the small intestine of the guinea-pig. *Cell Tissue Res.* **285**, 149-156.

Song, Z. M., Brookes, S. J., Neild, T. O. and Costa, M. (1997a). Immunohistochemical and electrophysiological characterization of submucous neurons from the guinea-pig small intestine in organ culture. *J. Auton. Nerv. Syst.* **63**, 161-171.

Song, Z. M., Brookes, S. J., Ramsay, G. A. and Costa, M. (1997b). Characterization of myenteric interneurons with somatostatin immunoreactivity in the guinea-pig small intestine. *Neuroscience* **80**, 907-923.

Song, Z. M., Costa, M. and Brookes, S. J. (1998). Projections of submucous neurons to the myenteric plexus in the guinea pig small intestine. *J. Comp. Neurol.* **399**, 255-268.

Surprenant, A. and Crist, J. (1988). Electrophysiological characterization of functionally distinct 5- hydroxytryptamine receptors on guinea-pig submucous plexus. *Neuroscience* **24**, 283-295.

Takeda, D., Nakatsuka, T., Papke, R. and Gu, J. G. (2003). Modulation of inhibitory synaptic activity by a non-alpha4beta2, non-alpha7 subtype of nicotinic receptors in the substantia gelatinosa of adult rat spinal cord. *Pain* **101**, 13-23.

Tzartos, S. J., Rand, D. E., Einarson, B. L. and Lindstrom, J. M. (1981). Mapping of surface structures of electrophorus acetylcholine receptor using monoclonal antibodies. *J. Biol. Chem.* **256**, 8635-8645.

Tzartos, S., Hochschwender, S., Vasquez, P. and Lindstrom, J. (1987). Passive transfer of experimental autoimmune myasthenia gravis by monoclonal antibodies to the main immunogenic region of the acetylcholine receptor. *J. Neuroimmunol.* **15**, 185-194.

Vanner, S. (2000). Myenteric neurons activate submucosal vasodilator neurons in guinea pig ileum. *Am J. Physiol. Gastrointest. Liver Physiol.* **279**, G380-G387.

Vernino, S., Adamski, J., Kryzer, T. J., Fealey, R. D. and Lennon, V. A. (1998). Neuronal nicotinic ACh receptor antibody in subacute autonomic neuropathy and cancer-related syndromes. *Neurology* **50**, 1806-1813.

Vernino, S., Low, P. A. and Lennon, V. A. (2003). Experimental autoimmune autonomic neuropathy. *J. Neurophysiol.* **90**, 2053-2059.

Wang, F., Gerzanich, V., Wells, G. B., Anand, R., Peng, X., Keyser, K. and Lindstrom, J. (1996). Assembly of human neuronal nicotinic receptor alpha5 subunits with alpha3, beta2, and beta4 subunits. *J. Biol. Chem.* **271**, 17656-17665.

Wang, F., Nelson, M. E., Kuryatov, A., Olale, F., Cooper, J., Keyser, K. and Lindstrom, J. (1998). Chronic nicotine treatment up-regulates human alpha3 beta2 but not alpha3 beta4 acetylcholine receptors stably transfected in human embryonic kidney cells. *J. Biol. Chem.* **273**, 28721-28732.

Wang, N., Orr-Urtreger, A., Chapman, J., Rabinowitz, R. and Korczyn, A. D. (2003). Deficiency of nicotinic acetylcholine receptor beta 4 subunit causes autonomic cardiac and intestinal dysfunction. *Mol. Pharmacol.* **63**, 574-580.

Whiting, P. J. and Lindstrom, J. M. (1988). Characterization of bovine and human neuronal nicotinic acetylcholine receptors using monoclonal antibodies. *J. Neurosci.* **8**, 3395-3404.

Whiting, P. J., Schoepfer, R., Conroy, W. G., Gore, M. J., Keyser, K. T., Shimasaki, S., Esch, F. and Lindstrom, J. M. (1991). Expression of nicotinic acetylcholine receptor subtypes in brain and retina. *Brain Res. Mol. Brain Res.* **10**, 61-70.

Zhou, X. and Galligan, J. J. (1999). Synaptic activation and properties of 5-hydroxytryptamine(3) receptors in myenteric neurons of guinea pig intestine. *J. Pharmacol. Exp. Ther.* **290**, 803-810.

Zhou, X., Ren, J., Brown, E., Schneider, D., Caraballo-Lopez, Y. and Galligan, J. J. (2002). Pharmacological properties of nicotinic acetylcholine receptors expressed by guinea pig small intestinal myenteric neurons. *J. Pharmacol. Exp. Ther.* **302**, 889-897.

Zins, B. J., Sandborn, W. J., Mays, D. C., Lawson, G. M., McKinney, J. A., Tremaine, W. J., Mahoney, D. W., Zinsmeister, A. R., Hurt, R. D., Offord, K. P. et al. (1997). Pharmacokinetics of nicotine tartrate after single-dose liquid enema, oral, and intravenous administration. *J. Clin. Pharmacol.* **37**, 426-436.